U.S. DEPARTMENT OF THE INTERIOR

U.S. GEOLOGICAL SURVEY

CHARACTERIZING FRACTURED ROCK FOR FLUID-FLOW, GEOMECHANICAL, AND PALEOSTRESS MODELING: METHODS AND PRELIMINARY RESULTS FROM YUCCA MOUNTAIN, NEVADA

By

C.C. Barton, Eric Larsen, W.R. Page, and T.M. Howard

Open-File Report 93-269

Prepared in cooperation with the
Nevada Operations Office
U.S. Department of Energy
(Interagency Agreement DE-AI08-78ET44802)

Denver, Colorado
1993

CONTENTS

PLATE

(Plate is in pocket)

FIGURES

TABLES

Characterizing Fractured Rock for Fluid-flow, Geomechanical, and Paleostress Modeling: Methods and Preliminary Results from Yucca Mountain, Nevada

By C.C. Barton, U.S. Geological Survey; Eric Larsen, formerly with Fenix & Scisson, Inc.; W.R. Page, U.S. Geological Survey; *and* T.M. Howard, formerly with Fenix and Scisson, Inc.

Abstract

Fractures have been characterized for fluid-flow, geomechanical, and paleostress modeling at three localities in the vicinity of drill hole USW G-4 at Yucca Mountain in southwestern Nevada. A method for fracture characterization is introduced that integrates mapping fracture-trace networks and quantifying eight fracture parameters: trace length, orientation, connectivity, aperture, roughness, shear offset, trace-length density, and mineralization.

A complex network of fractures was exposed on three 214- to 260-m^2 pavements cleared of debris in the upper lithophysal unit of the Tiva Canyon Member of the Miocene Paintbrush Tuff. The pavements are two-dimensional sections through the three-dimensional network of strata-bound fractures. All fractures with trace lengths greater than 0.2 m were mapped and studied.

The networks consist of two fracture types. The first type is distinguished by low surface-roughness coefficients and by open, anastomosing, matched half-tubes on opposing fracture faces. These fractures show only face separation without shear and are termed joints. Spherulites adjacent to joint faces suggest that the joints formed, opened, and their surfaces were quenched before or during devitrification of the tuff. The tubular structure is interpreted to be analogous to bread-crust structure on volcanic bombs. The cooling joints make up two well-defined sets striking 25 to 85° and 270 to 355°, both dipping perpendicular (plus or minus 6°) to foliation. Abutting of the two sets against each other suggests that they developed coevally. Both sets exhibit 3- to 5-m-wide swarms spaced 150-200 m apart. The second fracture type is distinguished by higher surface-roughness coefficients and by the absence of tubular structures on fracture faces. A few of these fractures have demonstrable shear offset and are thus termed faults. For most of these fractures, it was not possible to determine whether there was any shear displacement, and they are referred to as fractures. The fractures abut against and the faults offset the cooling joints and thus both postdate the joints. Unlike the cooling joints, the fractures do not define sets based on orientation or surface roughness.

The frequency distribution of surface-roughness coefficient (RC) for fractures and faults combined is fitted with a normal distribution and peaks at RC = 10. The RC frequency distribution for the cooling joints is also fitted with a normal distribution and peaks at RC = 2. The aperture frequency and trace-length frequency are best fitted by power laws. Anisotropy in aperture for the fracture networks is interpreted to result from a combination of tectonic and topographic stresses.

The spatial patchiness of fractures, joints, and faults in each of the networks is shown to be fractal, and the fractal dimensions D are 1.5, 1.4, 1.5.

INTRODUCTION

Purpose of Study

Fracture studies are part of the U.S. Geological Survey's effort to characterize the geologic and hydrologic framework at Yucca Mountain, Nevada (fig. 1). The site is currently being evaluated by the U.S. Department of Energy as a potential underground repository for high-level radioactive waste.

The impetus for this study is three-fold. First, hydrologic flow through fracture networks is a means

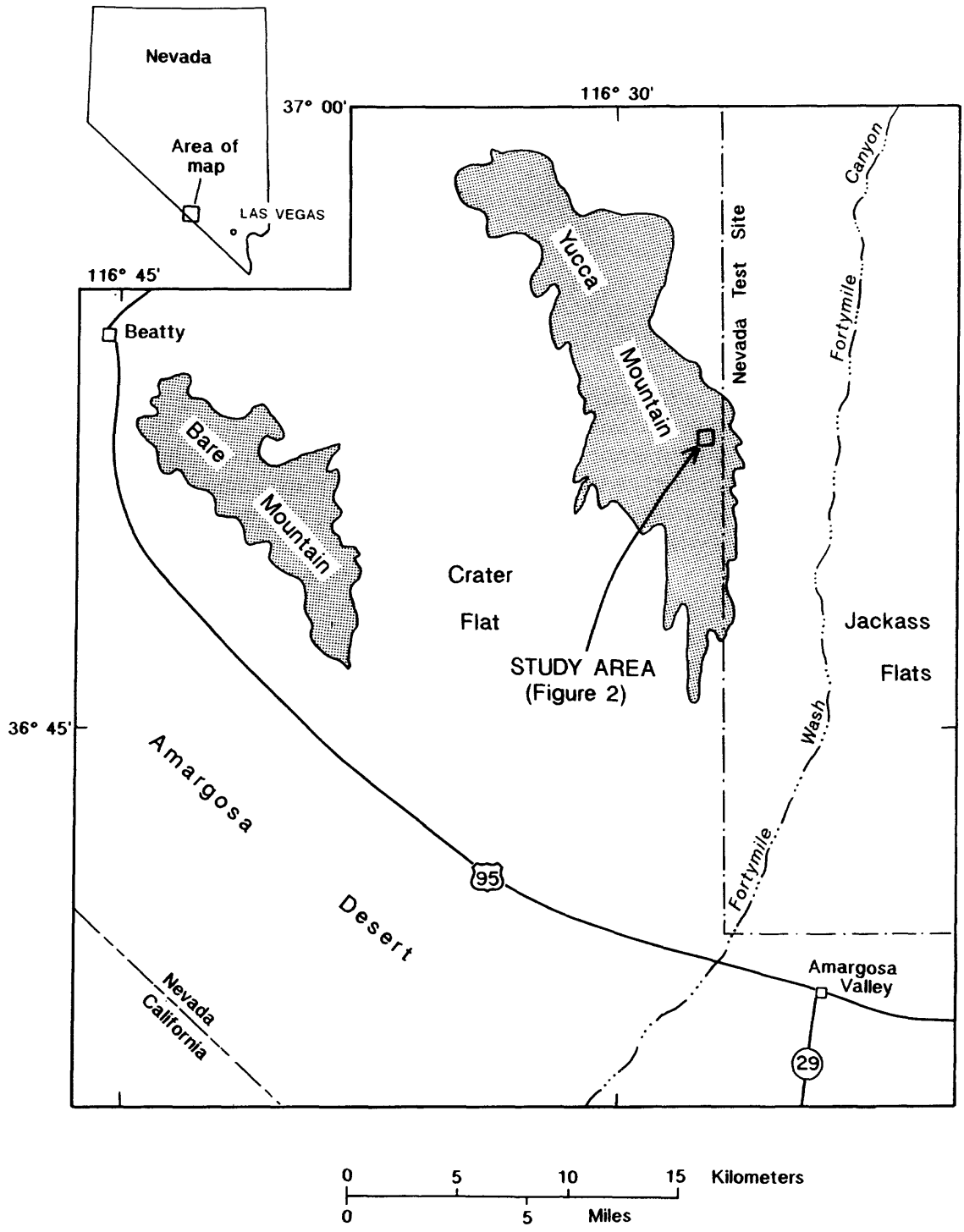

Figure 1. Index map showing location of study area at Yucca Mountain, southern Nevada.

by which water could reach buried radioactive waste and transport radionuclides out of the repository. Open networks are the primary avenues for gases and large fluxes of liquids through rock masses. In contrast to fracture-network flow, rock-matrix flow of water generally is significant only for small fluxes, such as are believed to predominate through much of the unsaturated-zone thickness in the volcanic tuffs at Yucca Mountain (Montazer and Wilson, 1984). However, fracture flow probably occurs episodically in the near-surface welded tuffs and reasonably could be expected under future climates similar to those of the Pleistocene, in this region. Saturated network permeabilities estimated from gas-injection tests in the tuffs are six to seven orders of magnitude greater than artificially saturated matrix permeabilities (Montazer and Wilson, 1984). Precipitation of minerals from aqueous solutions along fractures indicates that, in the geologic past, water has moved through Yucca Mountain along fractures.

Second, because the mountain is composed of fracture-bounded blocks over a wide range of size scales, the mechanical stability of the mountain during and after the construction of an underground repository depends in part on the geometry of the fracture networks.

Third, the fracture network is a composite of sequential fracture formation and reactivation events (Barton and others, 1986), which record parts of the paleostress history of the mountain.

Characterization of fractures for fluid-flow, geomechanical, and paleostress models now in use or under development cannot be achieved by what have been the standard geologic methods of study. The standard methods, such as those outlined in Kulander and others (1979), are based only on sampling natural outcrops and cores and do not include mapping of the fracture-trace patterns. While outcrop and core studies do permit characterization of orientation, aperture, and roughness, they do not permit characterization of trace length, spatial distribution, interconnectivity, or the size and shape of fracture-bounded blocks; all of which can be measured from a fracture-trace map of a pavement surface. All of the characteristics listed above are necessary for fluid-flow, geomechanical, and paleostress modeling.

Fracture networks in rock are volumetric, they partially fill volume space. Complete volumetric (three-dimensional) sampling over a wide range of length scales would be ideal, but is not technically possible nor physically practical. The pavements are two-dimensional sections through three-dimensional fracture networks. Cores are one-dimensional samples, and small outcrops are point samples which are zero-dimensional. The pavements permit sampling that is one integer dimension removed from the dimensionality of the networks. Core and outcrop samples are each further dimensionally removed.

Previous Mapping of Fracture Networks

Maps of fracture traces that adequately sample a fracture network are rare. The only such published maps that we are aware of are contained in four papers. Segall and Pollard (1983a and 1983b) mapped fracture traces on glacial pavements in the Mount Givens granodiorite in the Sierra Nevada of California. La Pointe and Hudson (1985) mapped fractures on a quarry floor in the Niagaran dolomite at Lannon, Wisconsin. Olson and Pollard (1989) mapped fracture traces in the Rico Limestone near Mexican Hat, Utah. All other published maps that we are aware of do not adequately sample the fracture network because one dimension of the map is too small, or because the range in fracture trace length mapped was too small. An optimal map would be equidimensional. Our own maps only approach this optimal shape. Therefore, in order to adequately sample the fracture network, we have mapped all fractures from the largest down to 0.2 m. We have sought to exclude weathering induced fractures and mapped only those fractures that we believe would be present in the same stratigraphic unit prior to exposure and weathering as described below.

Relevance of Pavement Method to Fluid-flow and Geomechanical Models

Contemporary fluid-flow and geomechanical models are generalized and utilize simulated networks (Long, 1983; Robinson, 1984; Long and others, 1985; Goodman and Shi, 1985; Lemos and others, 1985; Dershowitz and others, 1991). Site-specific models require site-specific fracture parameters. The method of pavement studies described below is the best basis for complete fracture characterization. The pavement method characterizes eight integrated fracture parameters. Published fluid-flow and geomechanical models are still too primitive to incorporate all of the parameters. The relevance of the parameters is discussed as they are introduced below, and foretells their incorporation in more sophisticated models in the future. It is not the intention of this report to present contemporary fluid-flow, geomechanical, or paleostress models or to detail how the fracture parameters discussed below are incorporated into such models. We encourage those interested in modeling to begin with the references cited at

the beginning of this paragraph. Our purpose is to introduce the reader to the relevant fracture characteristics and to methods by which they can be measured in the field and represented quantitatively.

Fracture Terminology

Fractures, joints, and faults form a three-dimensional interconnected network in nearly all rocks at or near the earth's surface. We use the terms, fracture, joint, and fault as follows. Fracture is the general term for a mechanically, chemically, or thermally induced planar or curviplanar parting in rock (excluding cleavage). Fractures whose opposing faces have demonstrable shear offset greater than the normal-opening are termed faults. Fractures whose opposing faces have demonstrable normal-opening offset (without shear or with shear less than the normal-opening) are termed joints. The term fracture is used below in the general sense where the offset cannot be determined and thus includes joints and faults, except where joints or faults are specified.

GEOLOGIC SETTING

Yucca Mountain is in the southern part of the Great Basin subprovince of the Basin and Range physiographic province. It is composed primarily of stratified Miocene volcanic ash-flow and ash-fall tuffs. The volcanic section locally ranges from about 1 to 4 km thick and lies unconformably, or perhaps in fault contact (Scott, 1986), on older Paleozoic sedimentary rocks. The complete volcanic stratigraphic section exposed at Yucca Mountain is described in Scott and Bonk (1984). All three pavements are in the densely welded, upper lithophysal unit of the Tiva Canyon Member of the Miocene Paintbrush Tuff. The source of the 13-Ma (R. B. Scott, U.S. Geological Survey, oral commun., 1986) Tiva Canyon tuffs is thought to be the Claim Canyon caldera, 2 km to the north (Byers and others, 1976).

Basin and Range extension began about 40 Ma in the region north of Yucca Mountain and was widespread in the southern Great Basin throughout Miocene time, 24 to 5 m.y. ago (U.S. Geological Survey, 1984). Structurally, Yucca Mountain consists of a series of elongate north-trending blocks bounded by major west-dipping normal faults, along which the blocks have been tilted eastward. Swarms of steeply dipping normal faults, each with small offset (normally less than 10 m), are common in the southern half of the mountain (Scott, 1984). The central part of the mountain is relatively unfaulted. The northern end of the mountain is cut diagonally by four northwest-trending valleys, probably strike-slip faults, possibly formed as part of the Las Vegas Valley-Walker Lane shear deformation (Scott and others, 1984).

Many of the normal faults on Yucca Mountain and in the region exhibit obliquely pitching striations on slickensided surfaces (R. B. Scott, U.S. Geological Survey, oral commun., 1989). If the striations are due to reactivation of the faults, then the implication is that the direction of regional extension has not remained fixed, but rather has moved within the northwest-southeast quadrants through time.

The study area is located in the central part of the mountain (fig. 1). We remapped the volcanic stratigraphy of Scott and Bonk (1984) in the study area (fig. 2) using altimeters to accurately plot stratigraphic contacts directly on a metric topographic base (Wu, 1985). The units are those defined and described by Scott and Bonk (1984). The only significant fault in the study area is the north-south-striking, steeply west-dipping Ghost Dance fault. The vertical offset on this normal fault decreases northward from about 8 m on the north side of Live Yucca Ridge to about 4 m on the south side of Dead Yucca Ridge (fig. 2). In the study area, the tuff foliation strikes 18°E and dips 8° southeast.

Location of Pavements

We prepared 1:50-scale maps of fracture traces at three sites in the immediate vicinity of drill hole USW G-4. The exposed bedrock pavements are designated 100, 200, and 300. Pavement 100 is on Live Yucca Ridge 500 m south of pavements 200 and 300, which are 15 m apart on Dead Yucca Ridge (fig. 2). The location of the pavements in Nevada state plane coordinates are: Pavement 100, N-765,345 E-561,870; Pavement 200, N-766,854 E-562,237; Pavement 300, N-766,854 E-562,362 (Science Applications International, 1988).

CLEARING AND MAPPING OF PAVEMENTS

In order to map the fracture networks, we cleared three nearly horizontal pavements to expose large areas of bedrock. The location of these pavements was governed by the desire to study fractures in the upper lithophysal unit, by the thinness of the debris layer to be removed (less than 12 cm at these locations), and by accessibility for the pumper truck used for hydraulic clearing. The size of each pavement was governed by the scale of the fracture pattern and thickness of debris

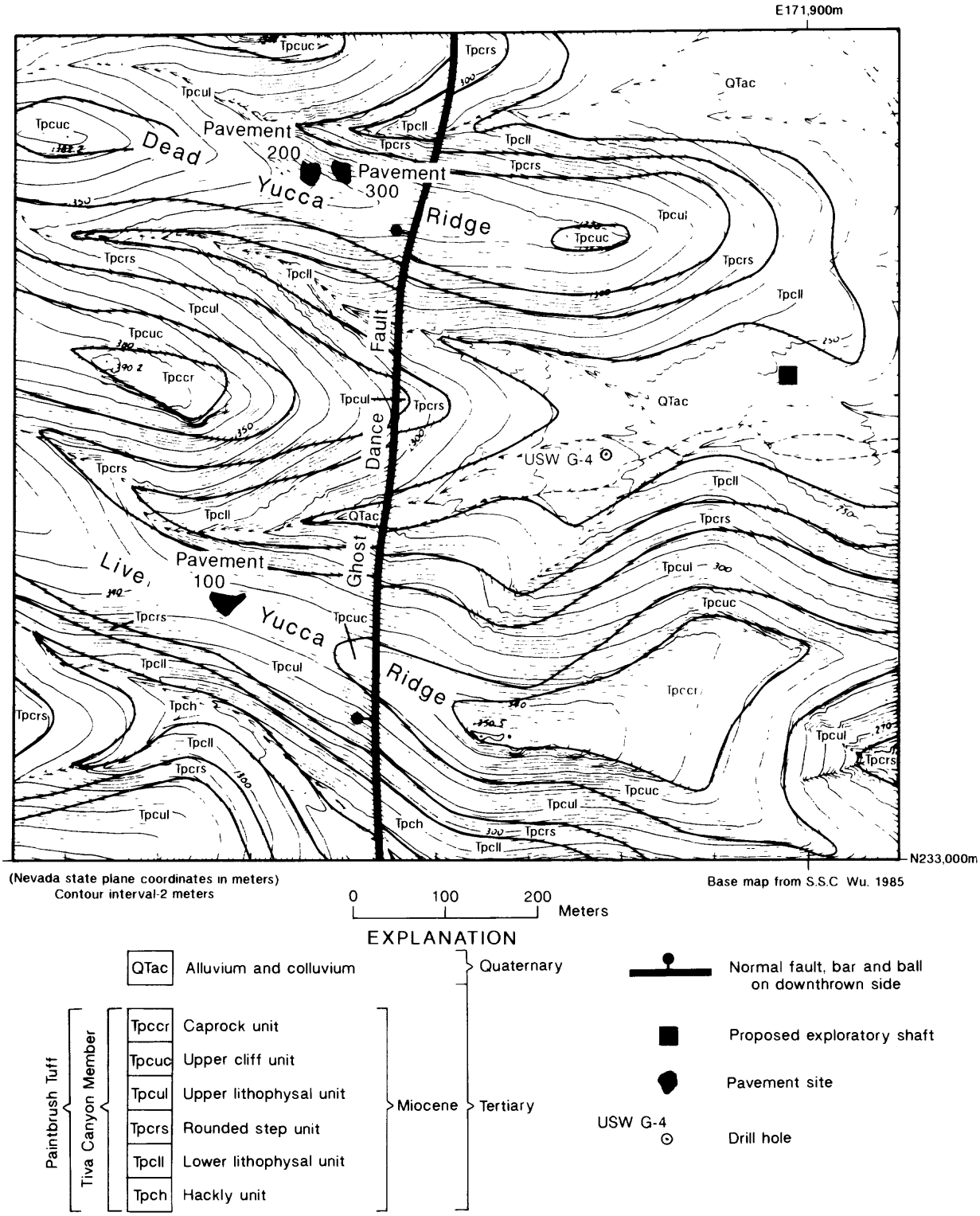

Figure 2. Geologic map of the area immediately surrounding drill hole USW G-4 showing the location of pavements 100, 200, and 300.

cover. Pavement 100 is 214 m^2 in area, pavement 200 is 260 m^2, and pavement 300 is 221 m^2.

Clearing of the pavements was done in two steps. First, all large boulders and brush were removed by hand. Second, rock debris and soil were removed using pressurized water sprayed from a firehose. The total volume of water used to clear these three pavements was 170 m^3 dispersed over an area of approximately 3,500 m^2. The area of dispersal is necessarily larger than the area of the pavements, because it includes the area of spray and runoff. Additional cleaning was done on a pavement using small brooms and brushes. The fracture network was thus completely exposed for mapping and study.

FRACTURE NETWORK MAPS

The bases for mapping the pavements were aerial photographs taken from a helicopter at an altitude of approximately 150 m. The orientation and scale of the bases were determined directly from 2-m-long, 0.22-m-wide arrows placed on the pavements and oriented to true north before the aerial photographs were taken. Where the aerial photograph was not normal to a pavement surface, we rectified the maps by redrafting them on large rubber sheets which were stretched over a wooden frame so as to uniformly remove distortion of the arrows and to restore lengths and angles between fractures on the map to those measured directly on the pavement. For all rectified maps, the resulting angle changes were less than four percent and length changes were less that three percent of the actual values measured directly on the pavements.

We mapped while standing on the pavements, adding fractures not visible on the aerial photographs. All fractures more than 0.2 m long were mapped on clear acetate sheets laid over the aerial photo bases. All fractures were mapped because we could not know which fractures were hydrologically significant. All fracture studies and maps necessarily must select some lower cutoff; we chose 0.2 meters for three reasons. First, the number of fractures increases with decreasing trace length as a power-law function, as can be seen on figure 12, the number of fractures increases dramatically below 0.2 m and approaches infinity as trace length goes to zero. The time required to map fractures would increase proportionately, and so we set 0.2 m as our lower cutoff in the interest of studying a number of pavements rather than focusing on just one. Second, a length of 0.2 m is approximately the lower limit of length that can be easily resolved on maps at the scale of publication. Third, at length scales shorter than 0.2 m there is a large population of fractures due to weathering which we sought to exclude from this study. We paid careful attention to mapping fracture intersections, abutments, and offset relationships. Because all fracture traces, intersections, and endings were mapped in detail on the pavement surface, the maps and data contained in this report are an uncensored sample of the exposed fracture population greater than 0.2 meters in trace length.

The pavement surfaces are not significantly weathered. Shallow dipping, bowl-shaped fractures exhibit fresh surfaces and therefore we consider them to be due to weathering, and they were excluded from this study. Fractures that are mineralized, coated, or stained were considered to be formed by geologic processes other than surface exposure and were included in our study. Calcrete deposits coat and infill all types of fractures exposed on the pavements, and so its presence was not used to discriminate between fractures due to weathering and those due to other geologic processes.

Plate 1 shows the maps for the three pavements. Each fracture is designated by a letter and number. The joints are designated by the letter J, and all other fractures by the letter F. Numbers with decimal fractions (for example, J40.1 on pavement 100) label individual segments of fractures that have been offset by later fractures. Numbers followed by a letter (for example, F60a and F60b on pavement 100) are used to label straight segments of fractures traces with strong curvature. Our segmentation of a strongly curved fracture trace into straight segments was done visually in order that the orientation of the fracture could be more accurately represented using strike and dip, a method which represents the fracture as a plane. In the quantitative studies of trace length presented below, the complete length of the curved fracture was used.

There are only four faults on pavement 100 and one each on pavements 200 and 300; they are included under the general category of fractures and identified in the comments section in the appendix because we could not determine whether they initially formed as joints or faults and because they are too few to constitute a statistically valid population. On the pavement maps they are identified as faults with arrows indicating the sense of offset (plate 1). No arrows are shown on fractures where the offset shown on the map is the result of local block-tilting, a minor readjustment due to plant and possibly ice wedging (for example, F25 on pavement 100). On all three maps, joints are shown by heavy lines and all other fractures by light lines. The azimuth of fracture strike, dip, dip direction, aperture, length, roughness coefficient, and the pitch of tubes on the face of cooling fractures are keyed to the maps by fracture number in the appendix. Areas of anomalously high infiltration are shown on plate 1 and are

described below in the section on fracture mineralization and alteration.

FRACTURE CHARACTERISTICS

Orientation

Fracture orientation has historically been considered the single most important characteristic. Where a number of fractures share a small range in orientation, they are said to form a set. As will be seen below, not all fractures at Yucca Mountain fall into well-defined sets. Also, not all fractures in a set were necessarily formed during the same event.

The orientation of each fracture was measured at the location where the fractures are numbered on the maps. The azimuth and dip were measured using a Brunton compass. Normally, the azimuth was measured on an exposed portion of the fracture face. In the few places where the rock locally is highly magnetized and deflection of the compass needle can result in incorrect azimuth readings taken when the compass is placed against a fracture, we place the compass against the fracture face and then move it away from the fracture face, parallel to the strike line, to waist level to take the reading.

Repeat measurements indicate that the azimuth readings are reproducible to 2°; dips are reproducible to 1°. The poles to fracture and joint planes and foliation for each of the pavements are plotted on lower-hemisphere equal-area projections on figures 3, 4, and 5. Figure 6 is a compilation of fractures and joints for all three pavements combined. The azimuths, dips, and dip directions are tabulated in the appendix. The fractures range in azimuth from 0 to 360° with slightly higher concentrations in the southeast and southwest quadrants; dips range from 46 to 90° with higher concentrations between 80 and 90°. The fractures cannot be grouped into well-defined sets based on orientation. The joints, in contrast, show clustered orientations and two sets can be defined. Joints of one set range in azimuth from 25 to 85° and in dip from 78 to 90°. Joints of the other set range in azimuth from 270 to 355° and in dip from 82 to 90°.

Fracture-Surface Roughness

Fracture-surface roughness is an important characteristic in hydrologic modeling because it influences the aperture variation as discussed below in the section on aperture, and thereby, the channeling of flow between the fracture walls. Roughness is important in geomechanics, also, for calculating the shear-strength of a fracture (Barton and Choubey, 1977) and closure stiffness under normal loads (Brown and Scholz, 1985). Roughness can also be useful in paleostress analyses as a basis for grouping fractures with a common mechanical and temporal origin, as will be shown below.

Fracture-surface roughness was measured where an unweathered portion could accommodate a 15-cm-long "shape copier." This device (fig. 7) is composed of 148 pins, each about 1 mm in width. The pins are held in place by frictional force between two rigid plates. The pins are movable so that when the copier is pressed against a fracture surface the pins move to mimic the surface. When the copier is removed from the surface, the pins retain the profile of the fracture roughness. Examples of fracture surface-roughness profiles taken from several fractures are shown on figure 8*A*. The roughness is expressed in the appendix by the roughness coefficient (RC). The RC was determined by visual comparison to a standard set of profiles of known RC (fig. 8*B*), which range (as integer values) from 0 to 20 (Barton and Choubey, 1977). We found that roughness measured in this way and at this scale generally does not vary plus-or-minus one RC unit with position or orientation on any given fracture surface and therefore only one measurement was made on each fracture. For segmented fractures, RC usually is the same or varies by only one integer value from segment to segment. We do note, that RC can differ by as much as five from segment to segment on segmented fractures (for example, fracture 11.1-11.2 on pavement 200). We offer no explanation of why roughness should vary from one segment to another, especially since the segments were once one continuous fracture.

Roughness frequencies are plotted on figures 9*A*, *B*, and *C* for each of the pavements. For segmented and highly curved fractures, an RC was measured for each segment or curved section, but the average for the segments or curved portions of a given fracture is plotted on the figures. RC ranges from 1 to 18 and is reproducible to plus-or-minus 2 coefficient values. The RC for the fractures and faults combined ranges from 3 to 18. The RC for the joints ranges from 1 to 4. In figure 9 we plot histograms of the frequency of roughness coefficient with bins of 2 coefficient values because that is the reproducibility of our measurement of RC. There is a bimodal distribution one for the joints and one for all other fractures. We fit each of the modes separately with normal distributions. The normal distribution curves are shown on figure 9. We did not attempt to fit any other type of distribution to the data, but based on visual inspection of the fit of the curves to the histo-

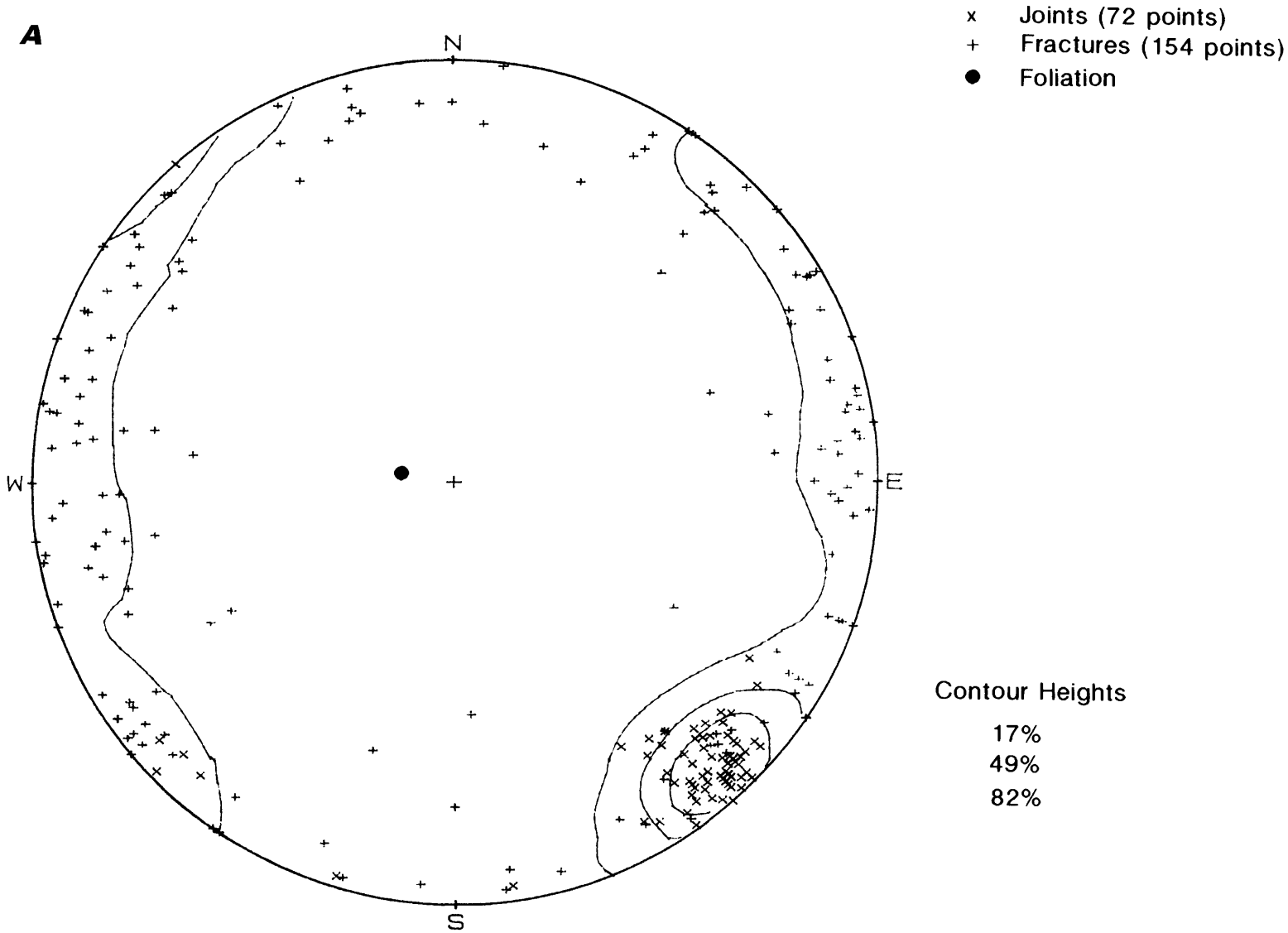

Figure 3A. Contoured lower-hemisphere equal-area projection of poles for pavement 100.

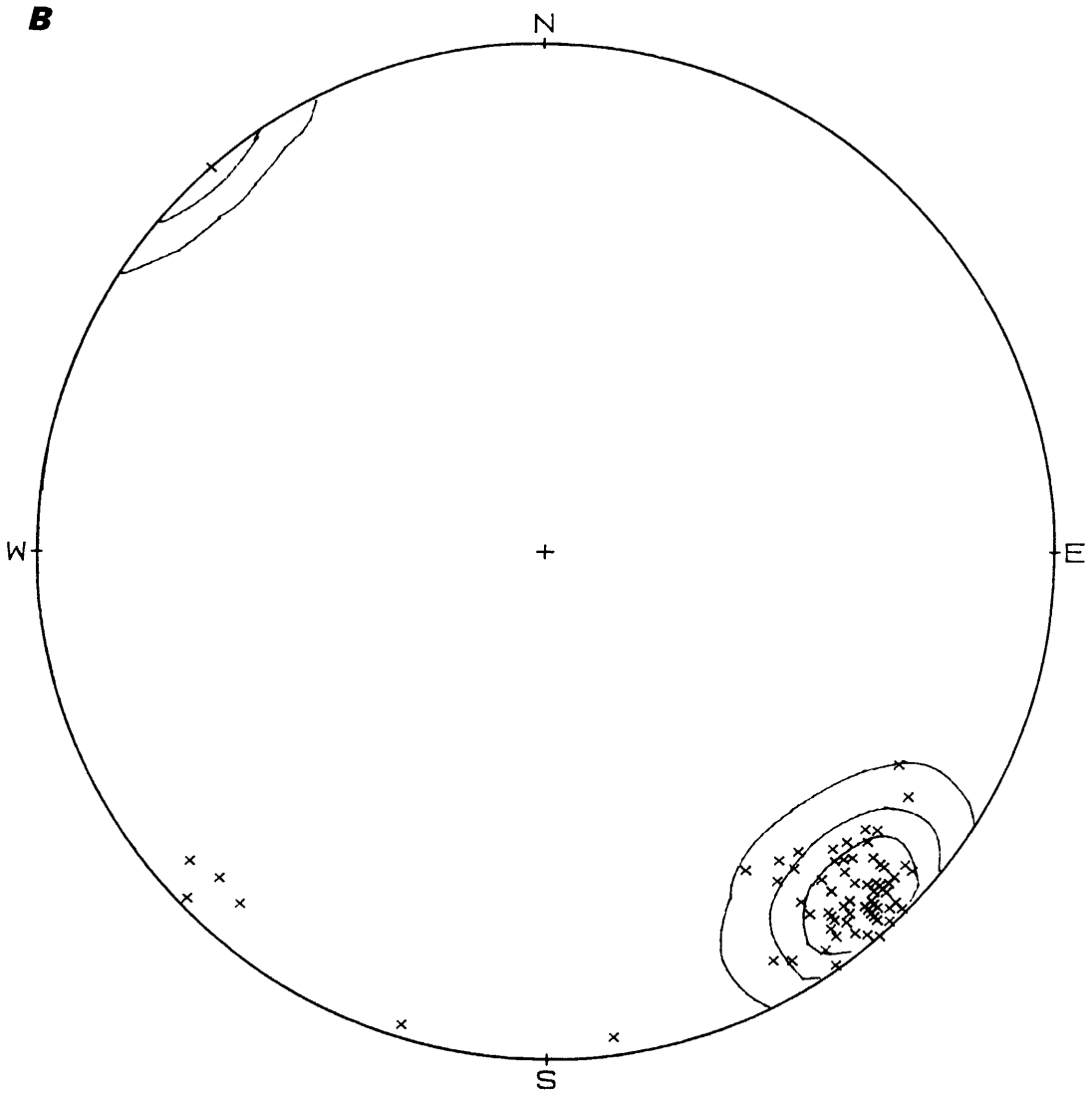

Figure 3B. Contoured lower-hemisphere equal-area projection of poles for pavement 100--Continued.

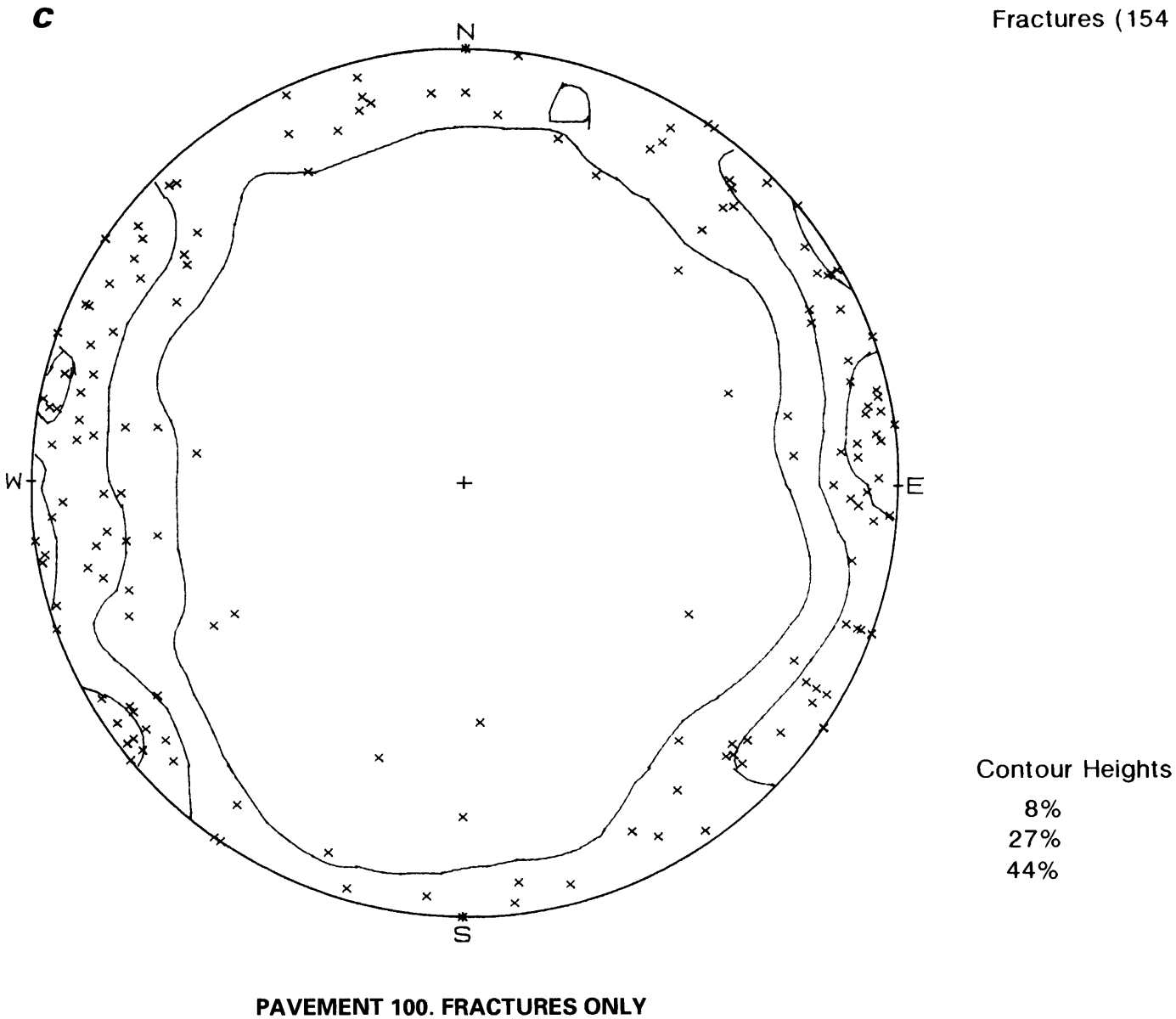

Figure 3. Contoured lower-hemisphere equal-area projection of poles for pavement 100--Continued.

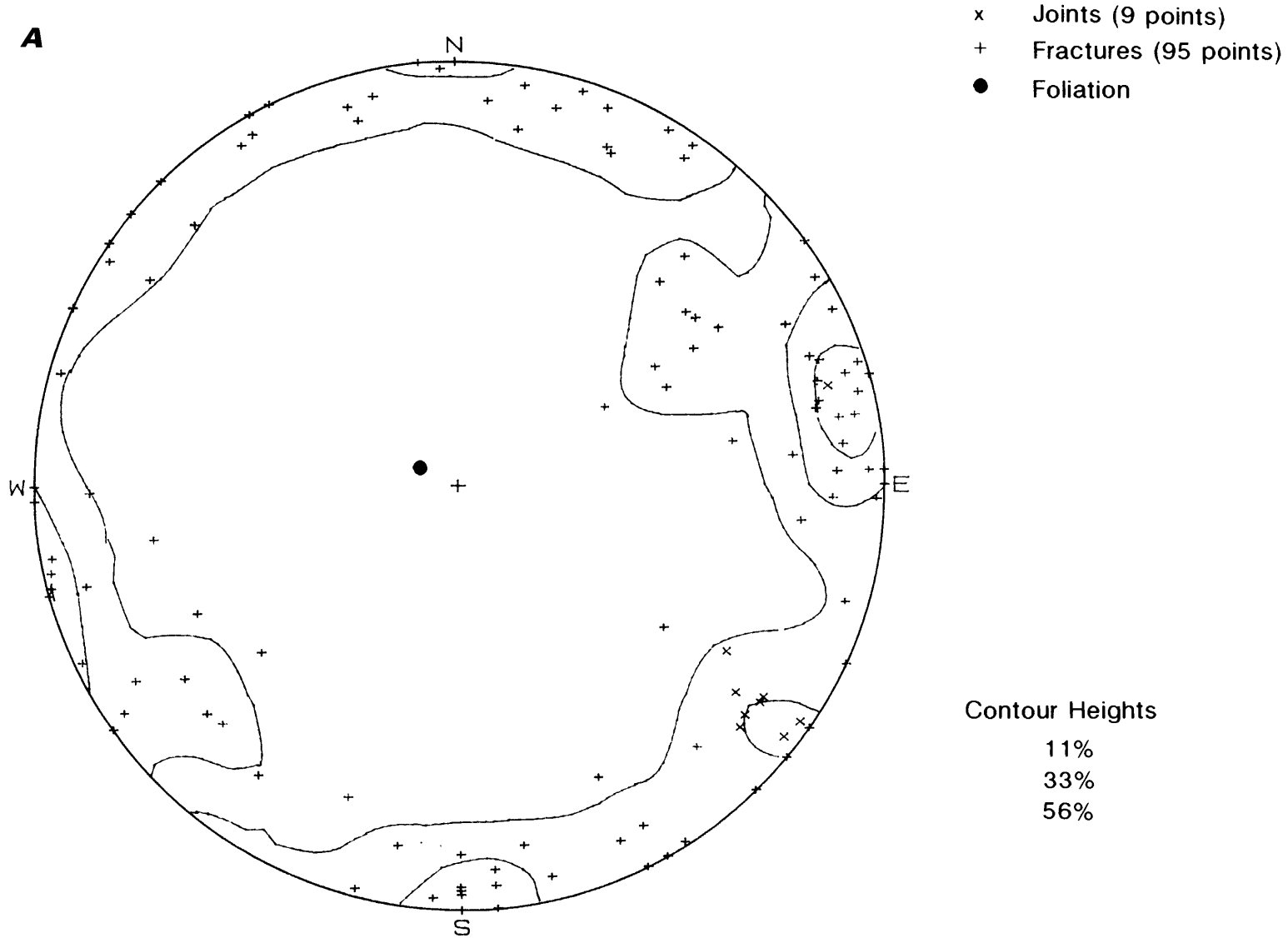

Figure 4. Contoured lower-hemisphere equal-area projection of poles for pavement 200.

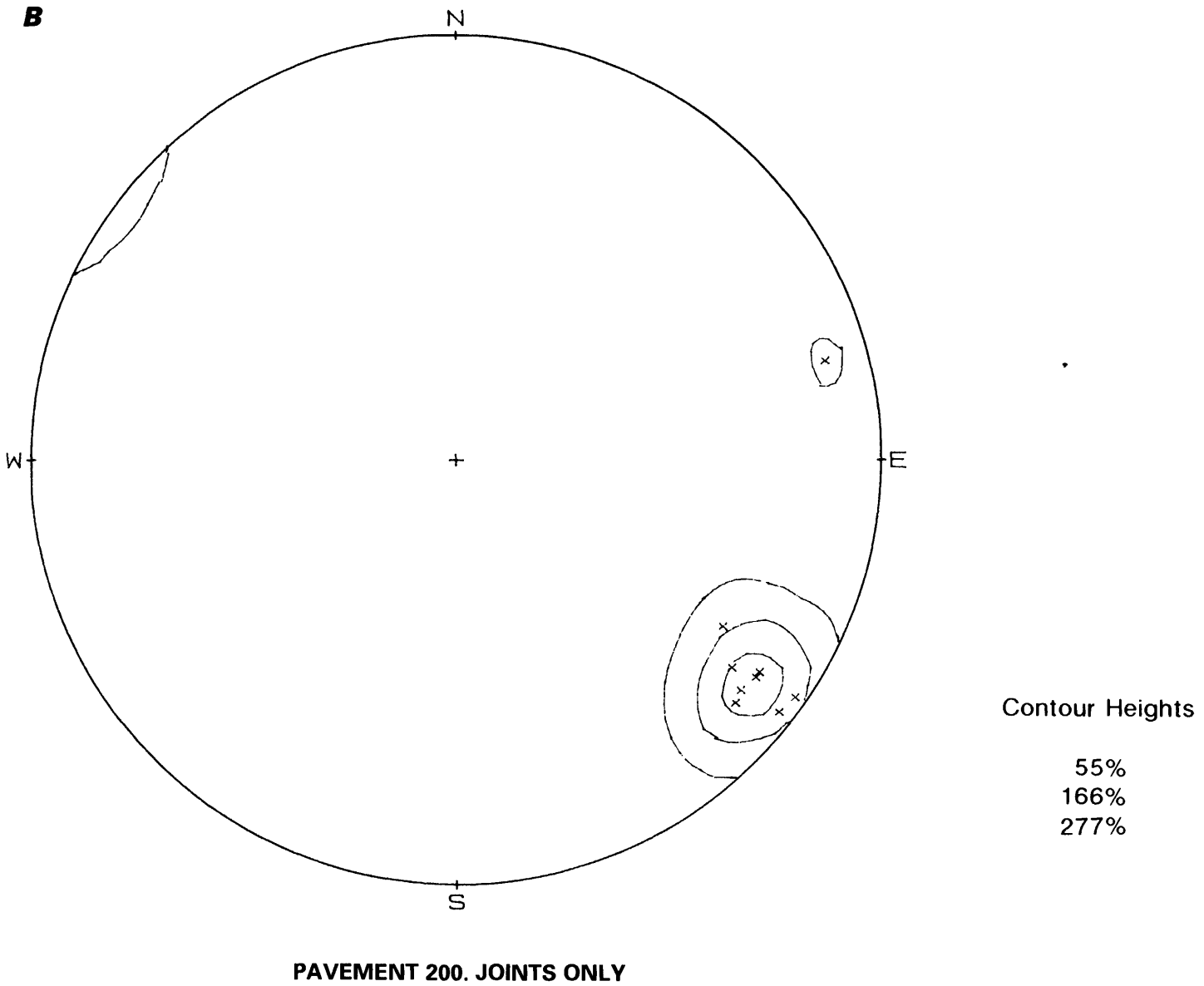

Figure 4B. Contoured lower-hemisphere equal-area projection of poles for pavement 200--Continued.

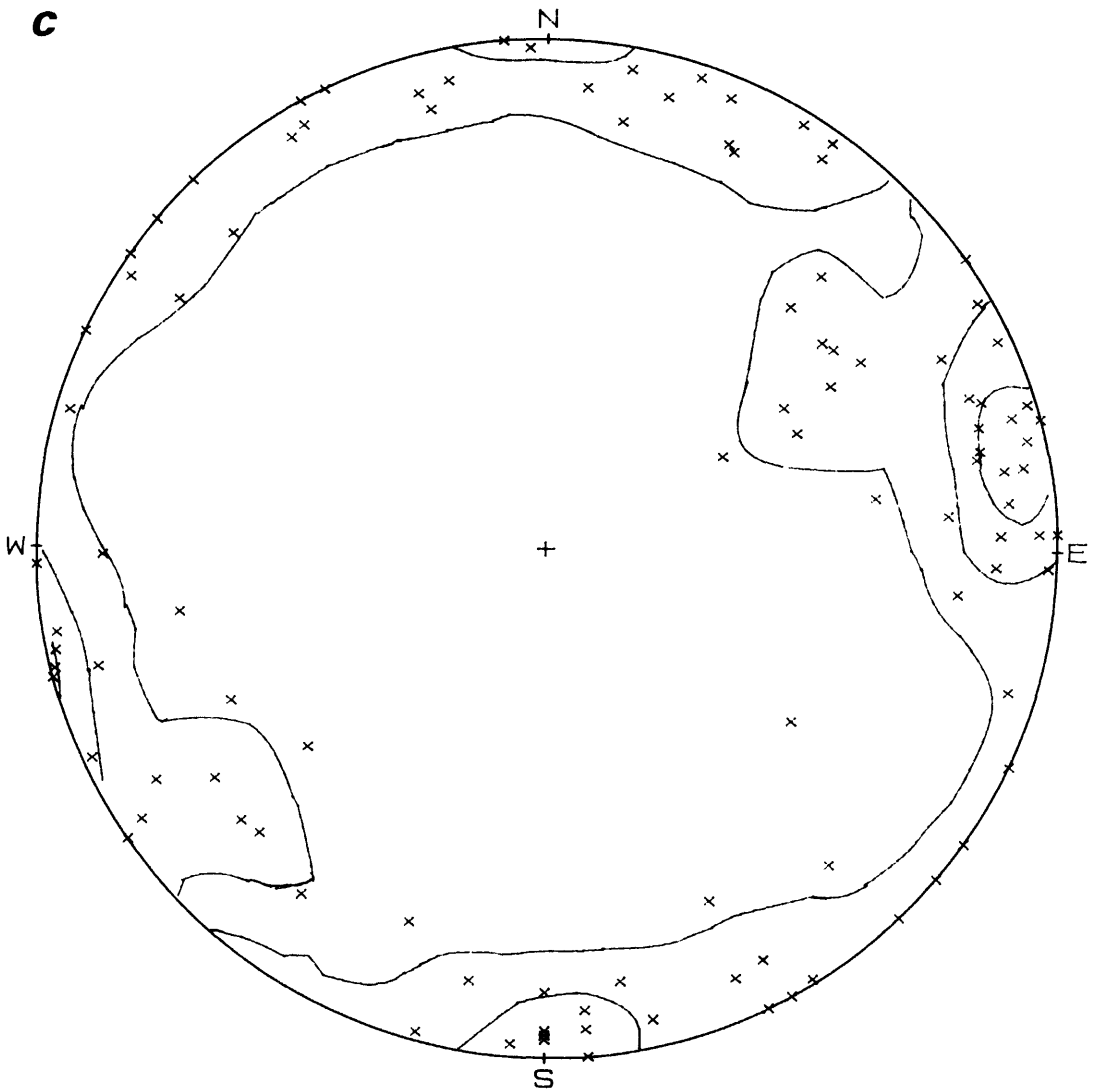

Figure 4C. Contoured lower-hemisphere equal-area projection of poles for pavement 200--Continued.

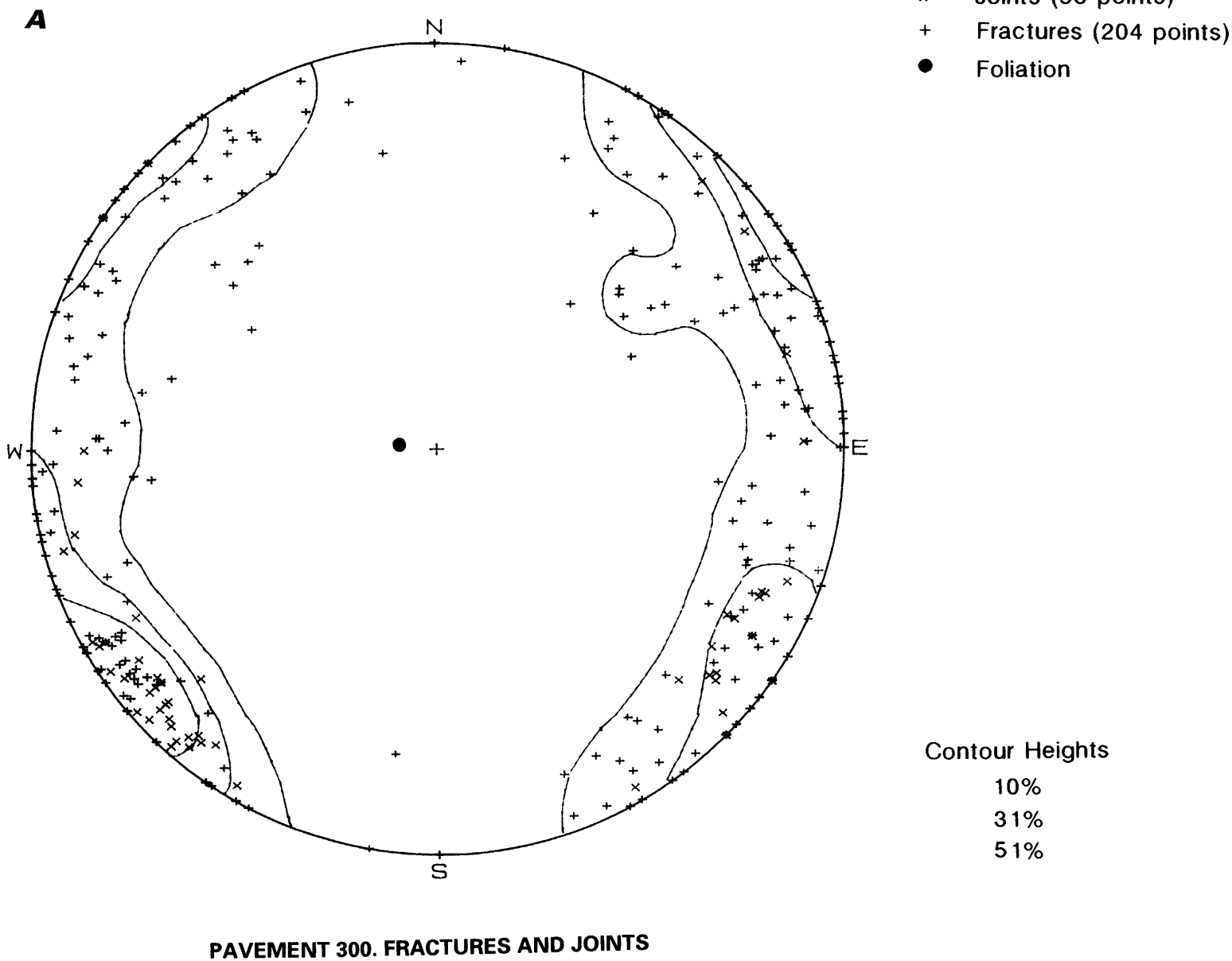

Figure 5A. Contoured lower-hemisphere equal-area projection of poles for pavement 300.

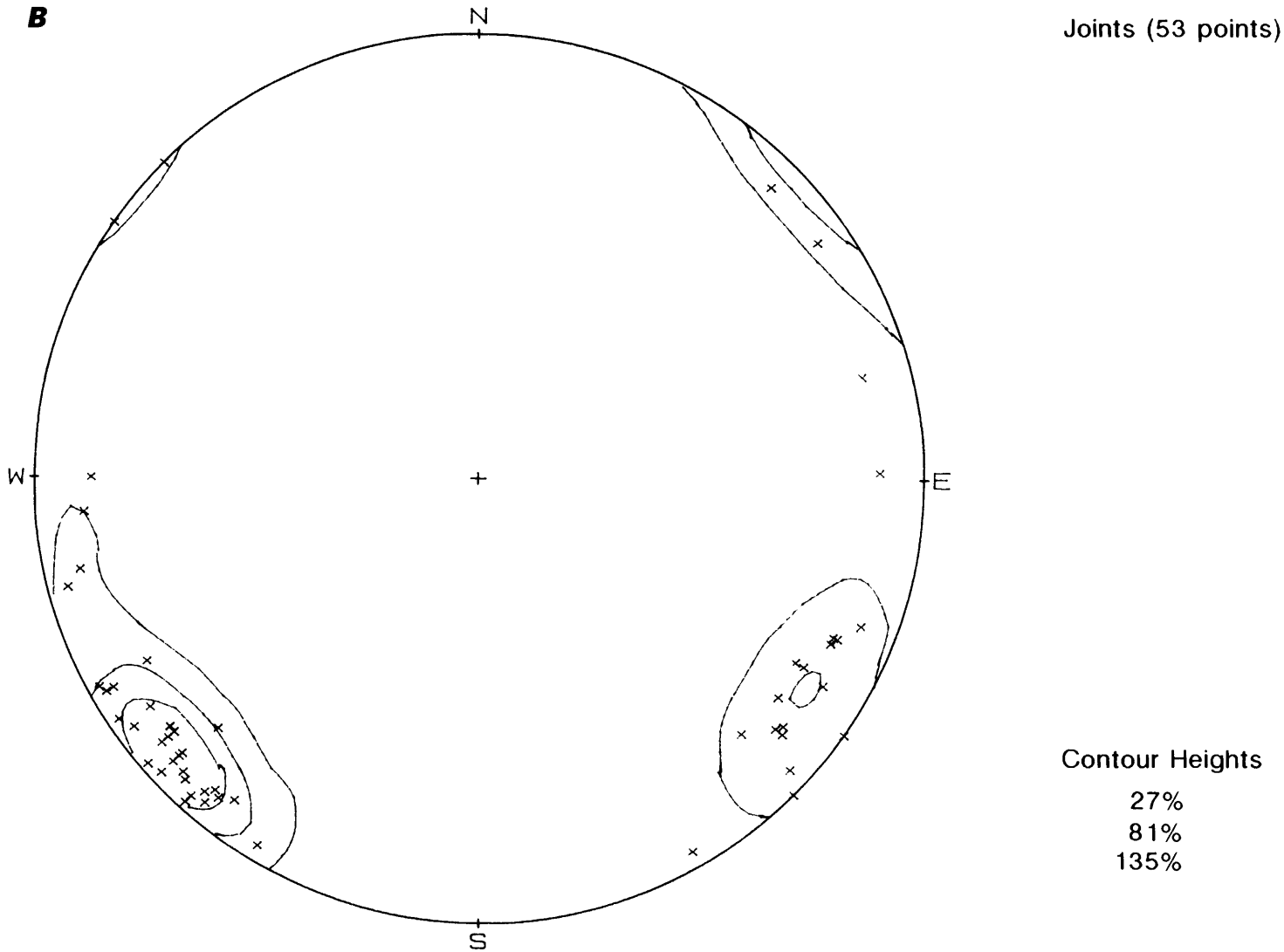

Figure 5B. Contoured lower-hemisphere equal-area projection of poles for pavement 300--Continued.

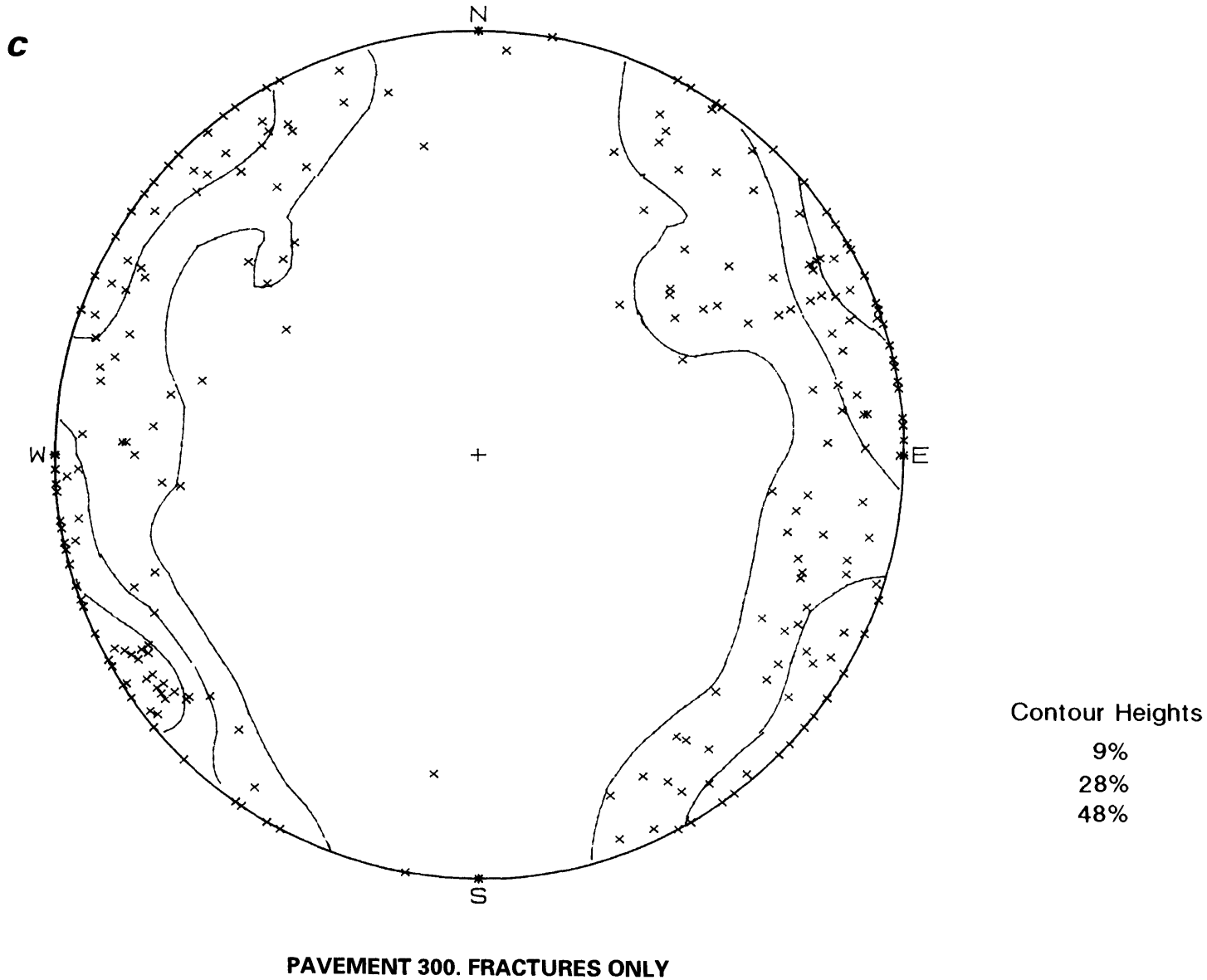

Figure 5C. Contoured lower-hemisphere equal-area projection of poles fpr pavement 300--Continued.

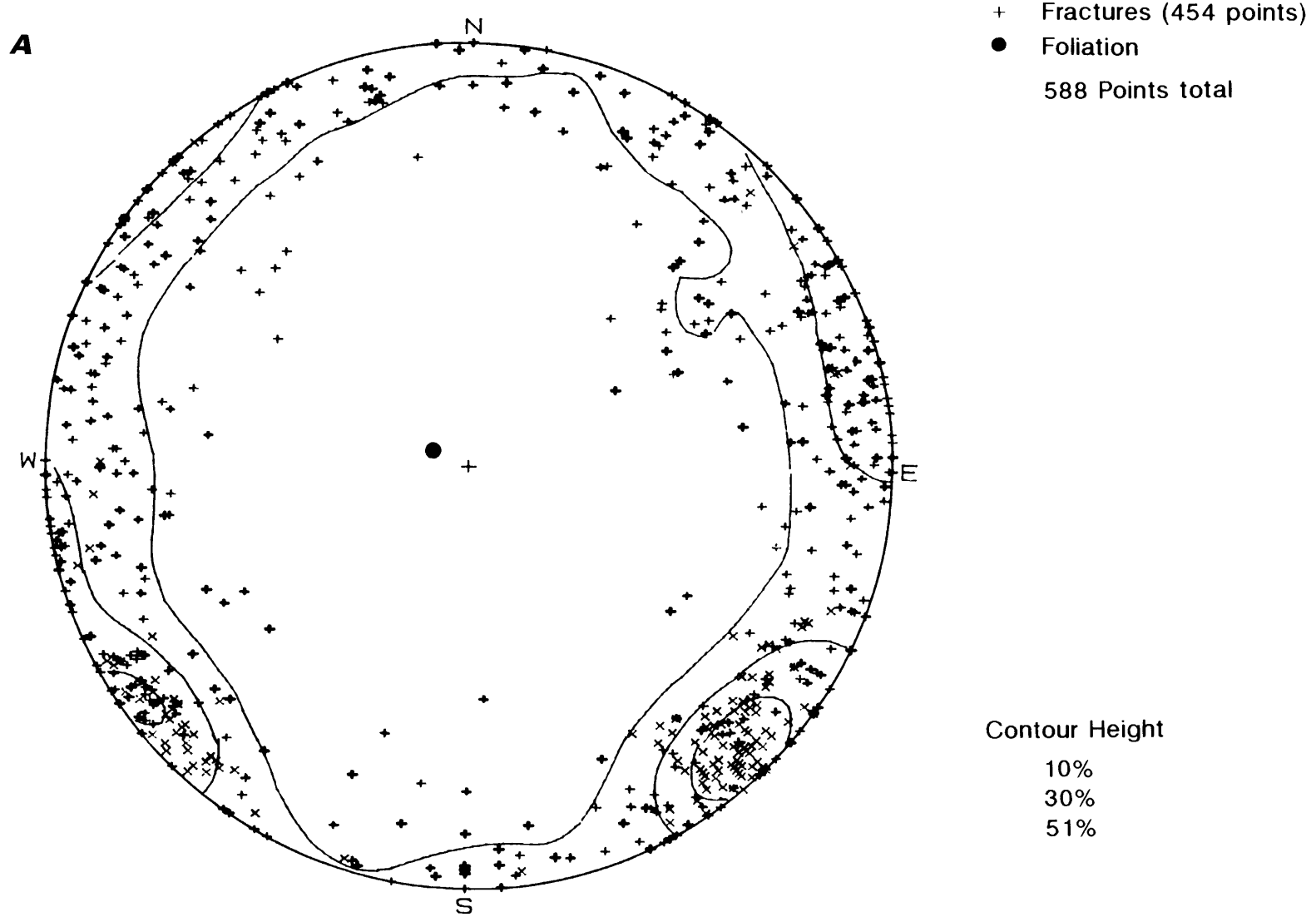

Figure 6A. Contoured lower-hemisphere equal-area projection of poles for pavements 100, 200, and 300 combined.

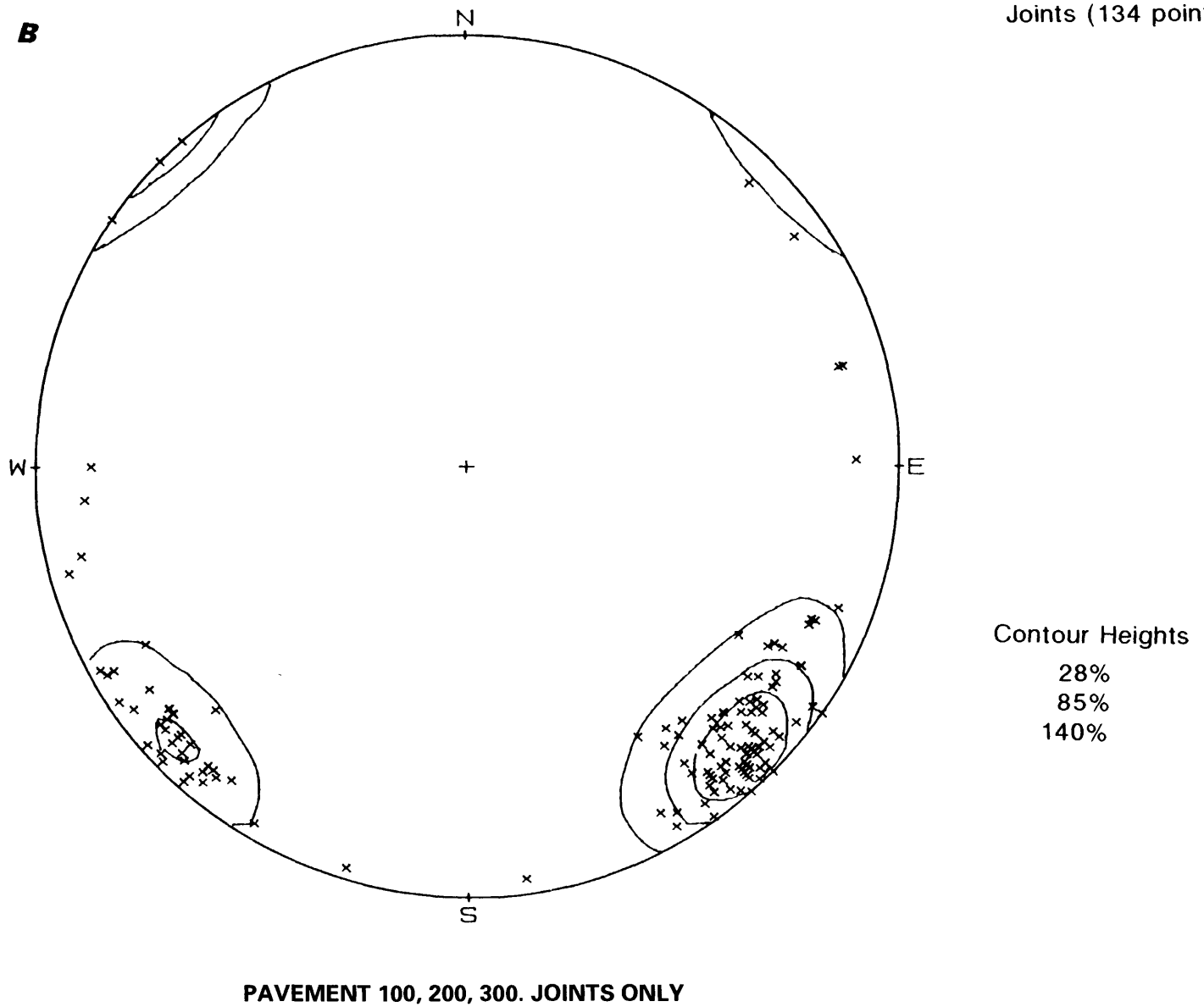

Figure 6B. Contoured lower-hemisphere equal-area projection for pavements 100, 200, and 300 combined--Continued.

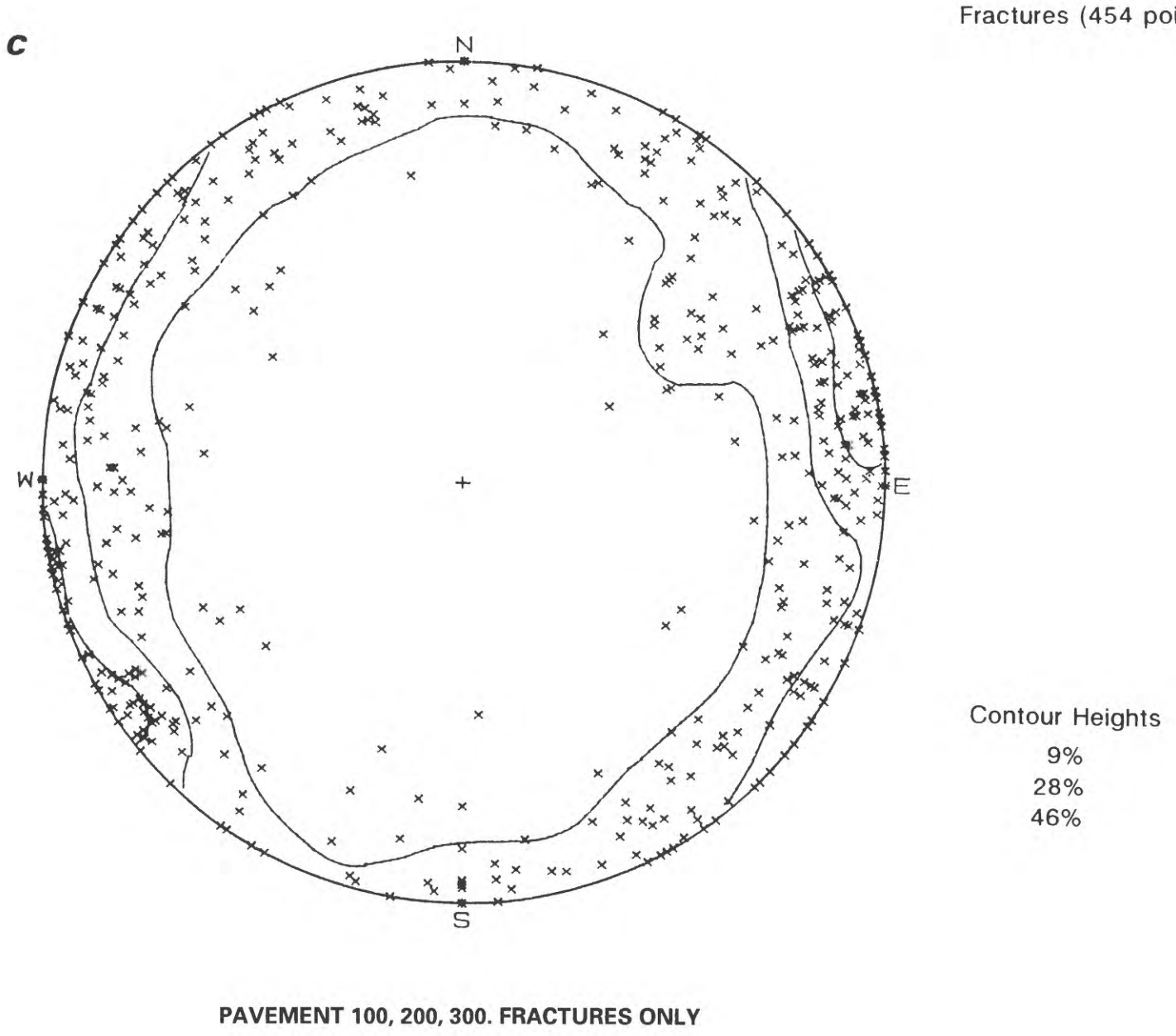

Figure 6C. Contoured lower-hemisphere equal-area projection of poles for pavements 100, 200 and 300 combined--Continued.

Figure 7. Photograph of "shape copier" used to record fracture surface roughness.

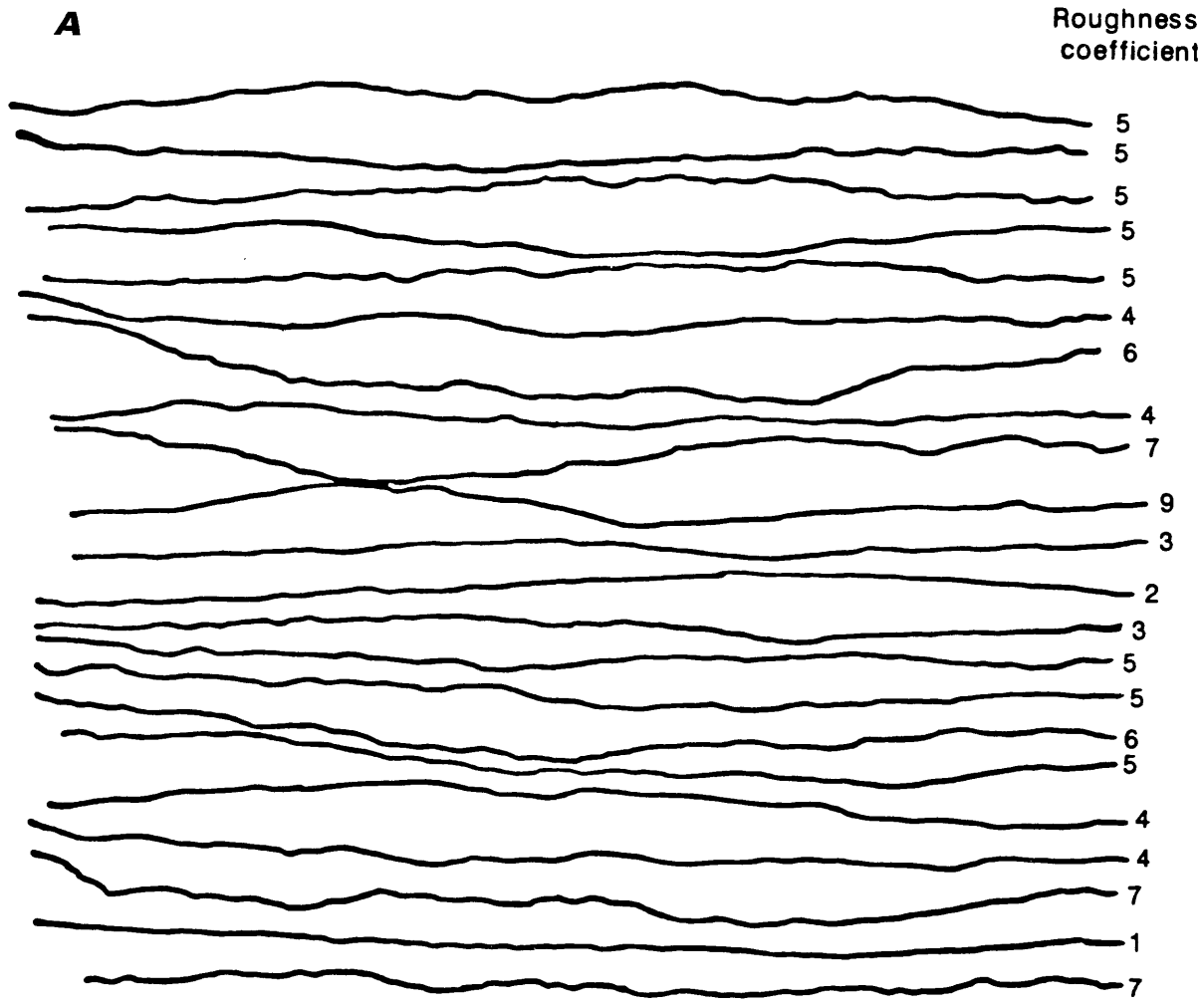

Figure 8A. Profiles of fracture -surface roughness.

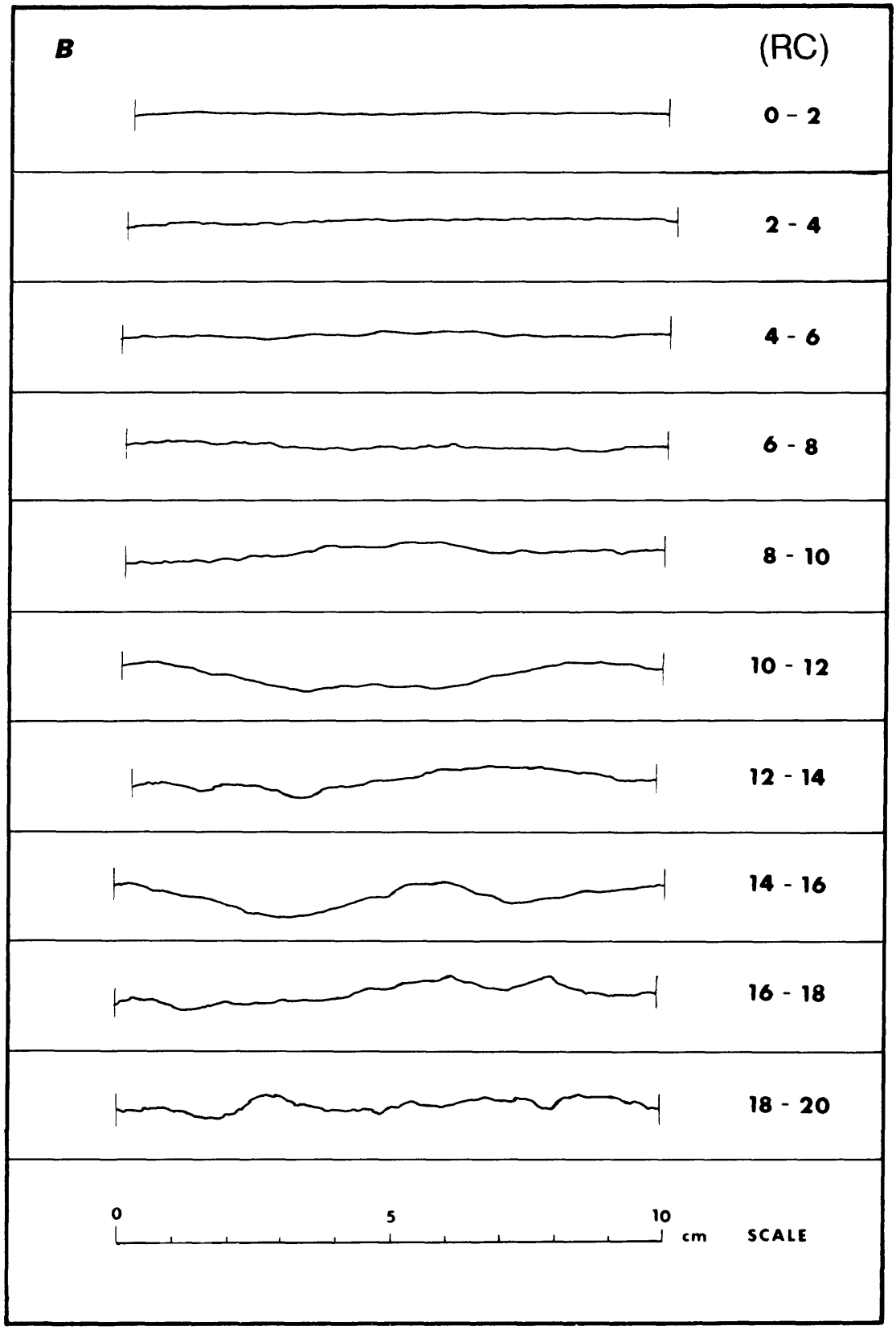

Figure 8B. Profiles of fracture-surface roughness (From Barton and Choubey, 1977, p. 19).

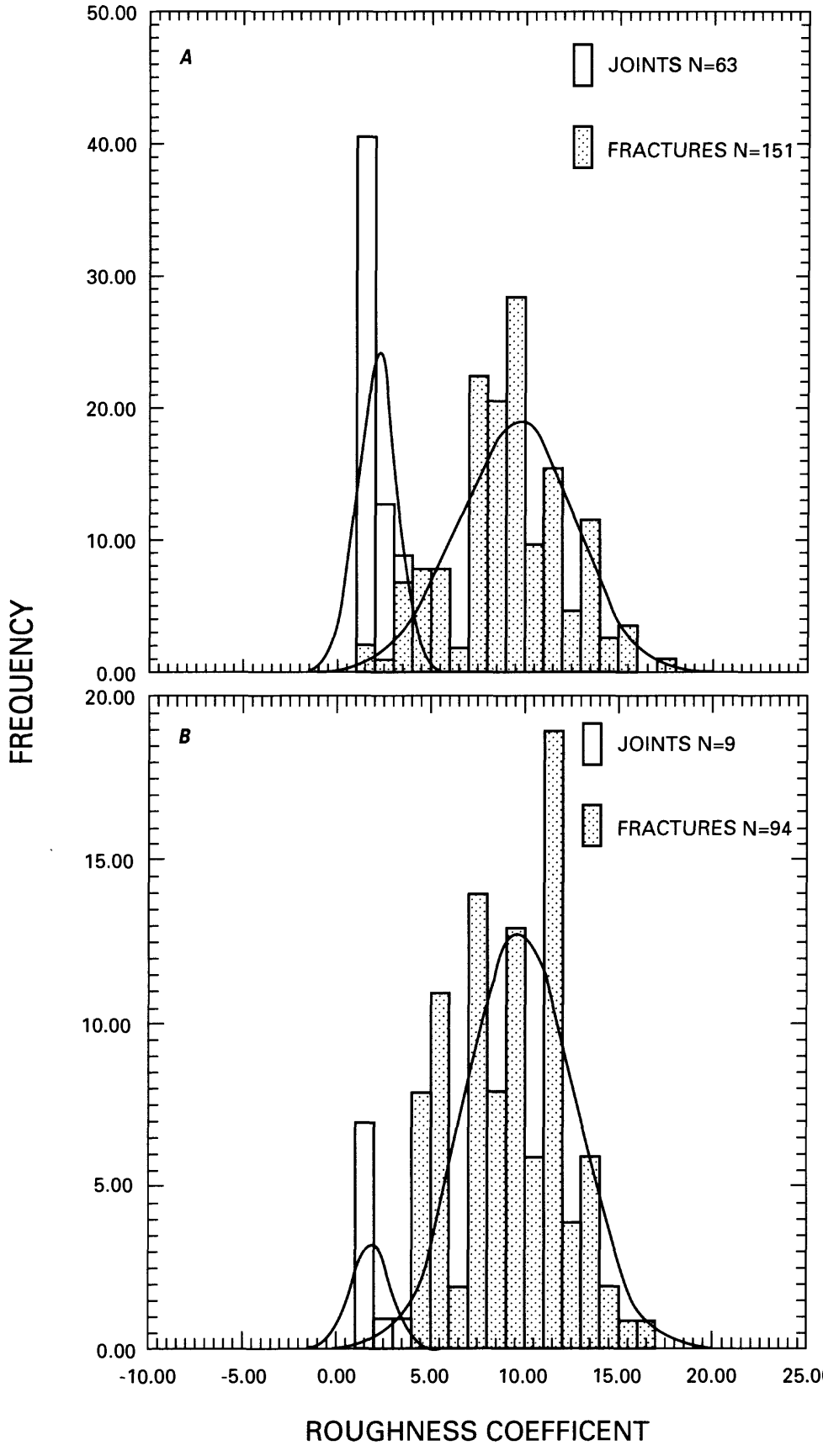

Figure 9A & 9B. Frequency histogram of roughness coefficient for joints and fractures fitted with normal curves. A. Pavement 100; B. Pavement 200; C. Pavement 300.

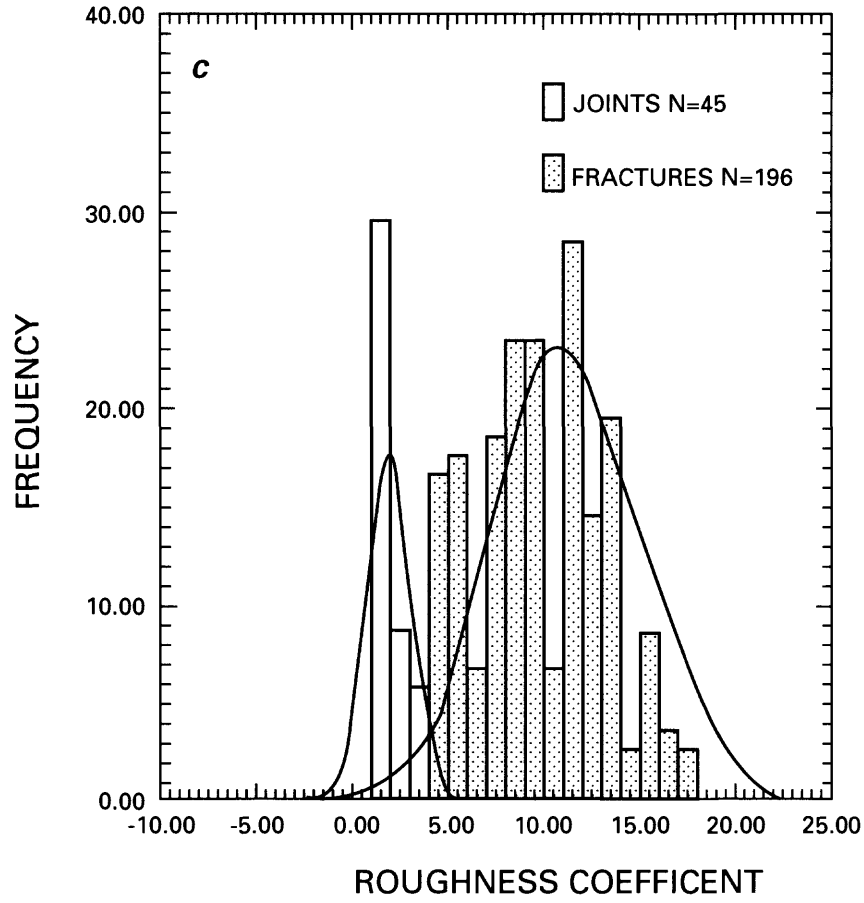

Firgure 9C. Frequency histogram of roughness coefficient for joints and fractures fitted with normal curves. A. Pavement 100; B. Pavement 200; C. Pavement 300--Continued.

grams, we suggest that RC for both the fractures and joints is normally distributed. Joints are less well fit, probably because their RC values are adjacent to a forbidden range (RC<0) and tail off toward higher values which produces asymmetric distributions. The histograms of frequency distributions (figure 9) are fit by normal curves of the form:

$$y = ((1/s)(2\pi)^{-1/2})\, e^{-(x-m)^2/2s} \quad (1)$$

where y is the frequency, x is the roughness coefficient, m is the mean, and s is the standard deviation. The values of the mean and standard deviation are given in table 1. The narrow range of RC for the joints suggests that the joints share a common mode and time of origin that is distinctly different from the fractures, as will be confirmed independently below.

Table 1. Normal-curve constants for fracture roughness coefficient

$$y = ((1/s)(2\pi)^{-1/2})\, e^{-(x-m)^2/2s}$$

(y = frequency, x = roughness coefficient, m = mean; s = standard deviation)

Pavement	Joints		Fractures	
	m	s	m	s
100	2.19	1.03	9.61	3.13
200	1.78	1.09	9.74	2.96
300	2.18	1.01	10.33	3.39
100, 200, 300 combined	2.16	1.03	9.96	3.22

Fracture Aperture

Aperture is extremely important in evaluating the flow characteristics of a fracture. For smooth-walled fractures, the volumetric flow rate is a function of the aperture cubed. For rough fractures, Cook (1992) reports that the volumetric flow rate in laboratory specimens of rock to be a function of the aperture to a power greater than three but less than six. The functional dependence of flow rate on aperture for rough fractures is a topic of much study at present, as is the functional relation between hydraulic aperture and mechanical aperture. Hydraulic aperture is a derived quantity, calculated from hydrologic tests performed either in the field of in the laboratory. We report here on the mechanical aperture measured on gaping fractures.

We recognize that the removal of overlying rock and exposure to surface weathering has affected the apertures. The exact values are affected, but not the form of the aperture distribution; we see the same form independent of hill slope, or location of the pavement as shown below. In contrast, apertures measured underground are affected by stress redistribution around the walls of boreholes and excavations, and by blasting. It is not possible to measure mechanical apertures that are unaffected, either at the surface or underground. Our view is that an imperfect measure of aperture is preferable to no measure.

A representative aperture was determined by visual inspection at places where weathering was minimal and mineralization absent. Small apertures were measured with an automotive feeler gage and larger ones with a ruler. Aperture frequencies, normalized by dividing the number in each interval by the total number measured on the pavement, are plotted on figure 10 for each pavement. We attempted to fit exponential, logarithmic, log-normal, and power-law functions to the histograms of aperture frequency. The histograms are best fit by a power law of the form $y = ax^b$, where y is the frequency, x is the aperture, and a and b are constants. The values of the constants and the coefficient of determination (goodness of fit) are given in table 2. At length scales less than the 0.2 meter lower cutoff in our data, we observe a dramatic increase in the number of fractures with decreasing size scale, down to the scale of micro-fractures. This observation further supports our conclusion that a power-law is the most appropriate fit to the aperture data.

Anisotropy in aperture for the network is of interest because it contributes to anisotropy in the hydraulic conductivity of the fracture network and in the bulk geomechanical properties. The apertures have opened in response to local and regional tectonic and topographic stresses that caused and subsequently reactivated the fractures. Apertures represent only the normal component of opening displacements.

In order to study aperture anisotropy as a function of orientation, we constructed a rose diagram to represent a two-dimensional summation of aperture as a function of the azimuth of fracture opening (fig. 11). The length of each petal in the diagram is the sum of apertures open in the direction of that 10° interval normalized by dividing by the number of fractures that contributed to that interval. The symmetry of the diagram is an artifact of considering all fractures to strike between 0 and 180° to first construct the right side of the diagram and then making the left side of the diagram symmetrical. The directions of slope of the pavement surfaces and the axes of ridges on which the pavements are located are also plotted on figure 11.

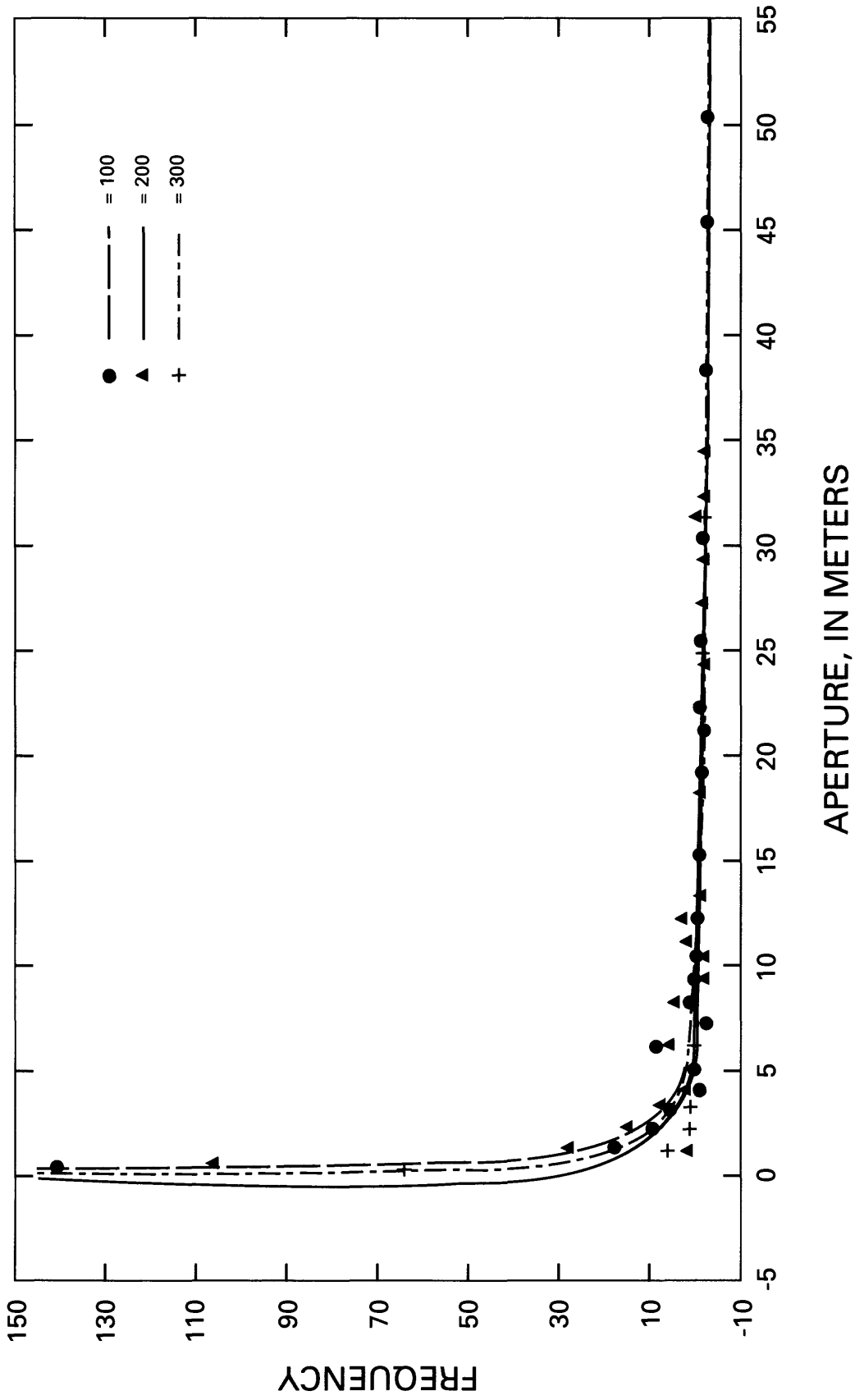

Figure 10. Frequency of fracture aperture for pavements 100, 200, and 300.

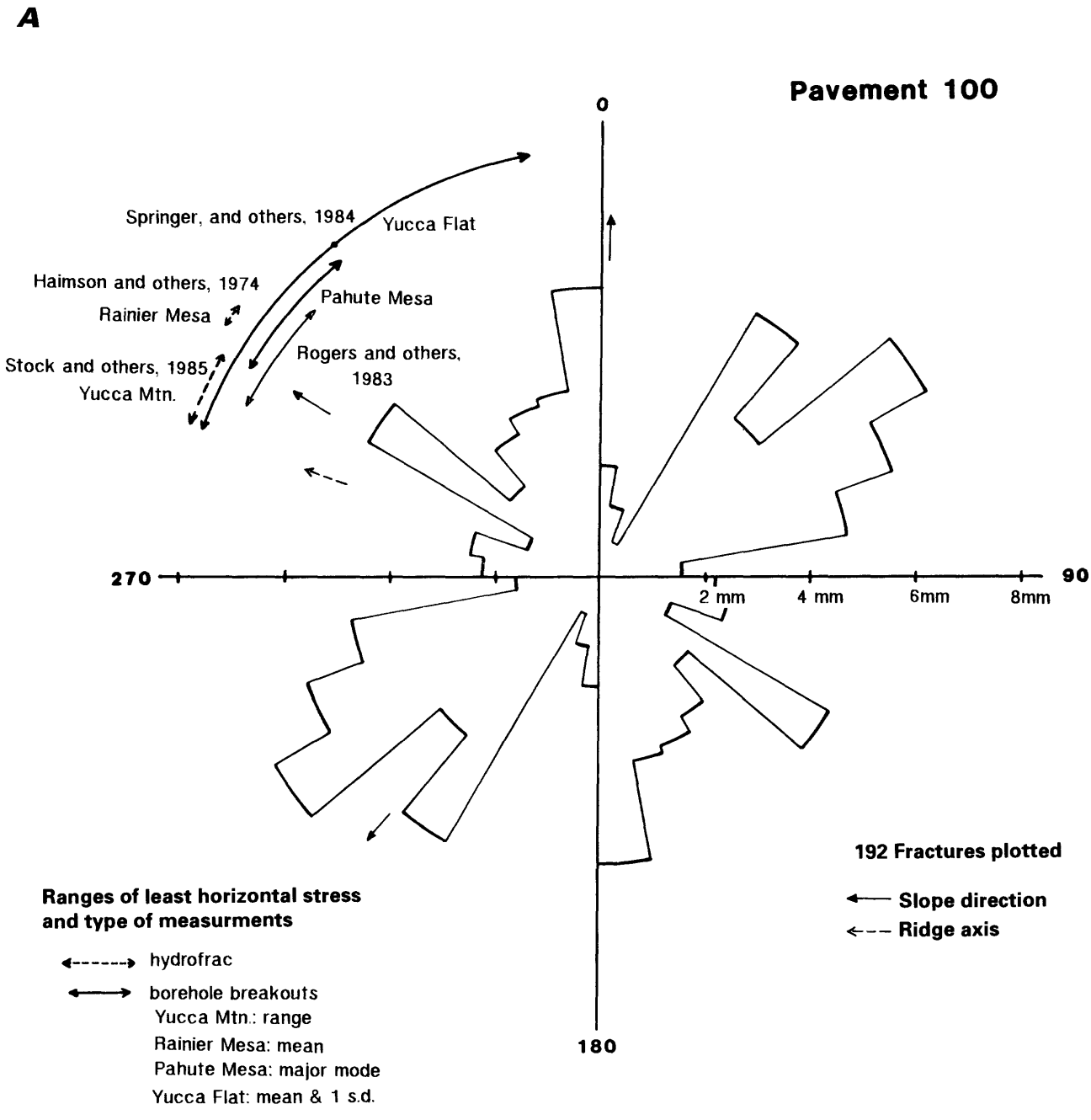

Figure 11A. Rose diagrams of aperture as a function of the azimuth of fracture opening. A. Pavement 100; B. Pavement 200; C. Pavement 300.

B

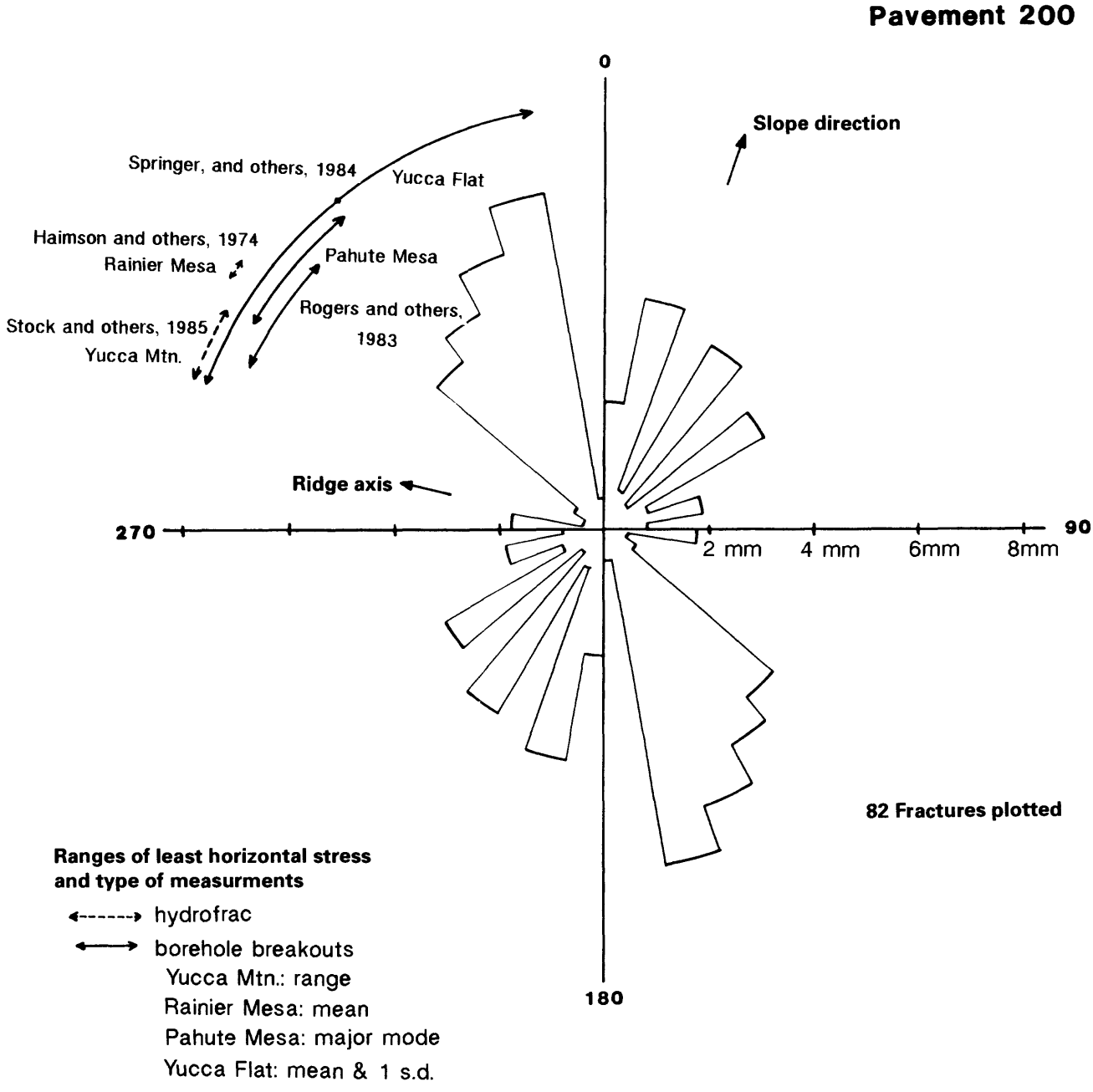

Figure 11B. Rose diagrams of aperture as a function of the azimuth of fracture opening. A. Pavement 100; B. Pavement 200; C. Pavement 300--Continued.

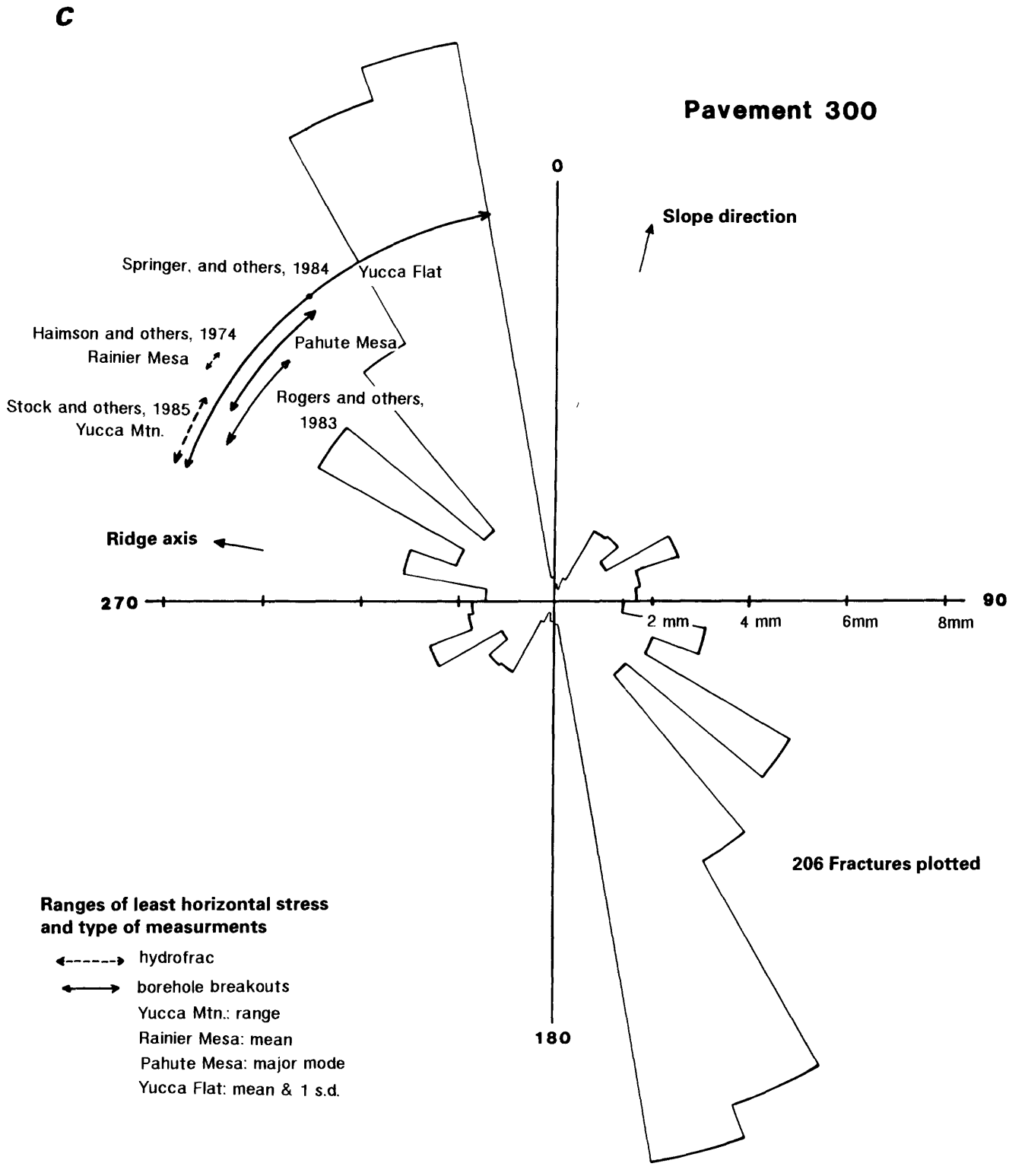

Figure 11C. Rose diagrams of aperture as a function of the azimuth of fracture opening. A. Pavement 100; B. Pavement 200; C. Pavement 300--Continued.

The slopes of pavement surfaces are less than twelve degrees and vary less than five degrees on any given pavement.

The azimuth of the least horizontal stress measured at or near Yucca Mountain by hydrofracture (Haimson and others, 1974; Stock and others, 1985) and borehole breakouts (Springer and others, 1984) are also plotted in figure 11. These methods indicate as much as 60° degrees of variation in the direction of the least horizontal stress, but it is always oriented in a northwest-southeast direction. This matches an analysis of earthquake focal mechanisms which sample deeper stratigraphic levels in the region (Rogers and others, 1983), and which resolves the least horizontal principal stress to be between 290 and 310°.

Inspection of figure 11 indicates anisotropy in fracture apertures, but interpretation is difficult. Azimuths of maximum opening on pavements 200 and 300 are northwest-southeast and fall within the range of the in-situ least horizontal stress, and therefore, we suggest that there may be a direct relation between the two. For pavement 100 (fig. 11*A*), the greatest opening direction is northeast-southwest which coincides with the direction of overall slope of the pavement surface, and therefore, we suggest that there may be a direct relation between the two.

Fracture-Trace Length

Fracture-trace lengths were measured on plate 1, and the frequencies, normalized by dividing the number in each interval by the total number measured on the pavement, are plotted on figure 12 for each of the three pavements. The plots include the exposed lengths of fractures whose traces extend beyond the edges of the pavement. Because these are distributions with long tails, truncation affects the exact values, but not the overall form of the distribution. The lower end of the distribution is truncated because no trace lengths less than 0.20 m were mapped. The upper end is truncated because many trace lengths exceed the dimensions of the pavements. As with aperture, we attempted to fit exponential, logarithmic, log-normal, and power-law functions to the trace-length frequency histograms. The histograms are best fit by a power law of the form $y = ax^b$, where y is the frequency, x is the trace length, and a and b are constants. The values of the constants and the coefficient of determination (goodness of fit) are shown in table 2. Qualitative observation of fractures less than our lower cutoff of 0.2 meters reveals greatly increasing numbers of fractures with decreasing size, this further supports a power-law distribution of fracture-trace lengths.

In order to test the validity of including fractures whose traces extend beyond the pavement boundary, we also fit the four types of functions to only those fractures completely contained within the pavement boundary. Again, the data for pavements 100, 200, and 300 were best fitted by a power law with the values of the power b within 9, 5, and 3 percent, respectively, of the values shown on table 2. Thus, we feel confident in including the traces of fractures that extend beyond the pavement boundary in statistical analyses of fracture trace length.

Segall and Pollard (1983) mapped fracture traces at two pavement sites in the Mount Givens granodiorite in the central Sierra Nevada Mountains of California. They also fit the trace-length frequency distributions with a power law. In order to compare our results with theirs, we have fitted their data following the method described above. For their data b equals -0.66 and -1.46. Our values of b range from -0.84 to -1.33 (table 2). In contrast to our study of networks composed of fractures of many generations and orientations, only one uniformly oriented generation is present at their sites. Also, the lower end of their distribution is truncated at 2 meters; ours continues down another order of magnitude to 0.2 meters. The same power-law form and similar values for the exponent b for both studies suggest that trace-length frequency may be controlled by geometric aspects of the fracture process that are independent of rock type, age, and tectonic history.

Qualitative examination of fracture traces down to 1 centimeter in length at the pavement sites revealed very high numbers of small fractures that are not visible to an observer from a standing position. Conversely, we have been able to follow the traces of some of the fractures for tens of meters beyond the boundaries of the pavements. These qualitative observations

Table 2. Power-law constants for trace length and aperture

$y = ax^b$

(r^2 = coefficient of determination)

(y = frequency; x = aperture a, b = constants)

Pavement	Trace length			Aperture		
	a	b	r^2	a	b	r^2
100	10.12	-1.17	0.78	15.78	-1.10	0.79
200	9.05	-0.84	.73	14.99	-0.87	.74
300	11.21	-1.32	.82	11.35	-0.99	.76
100, 200, 300 combined	12.17	-1.47	.84	15.36	-1.26	.82

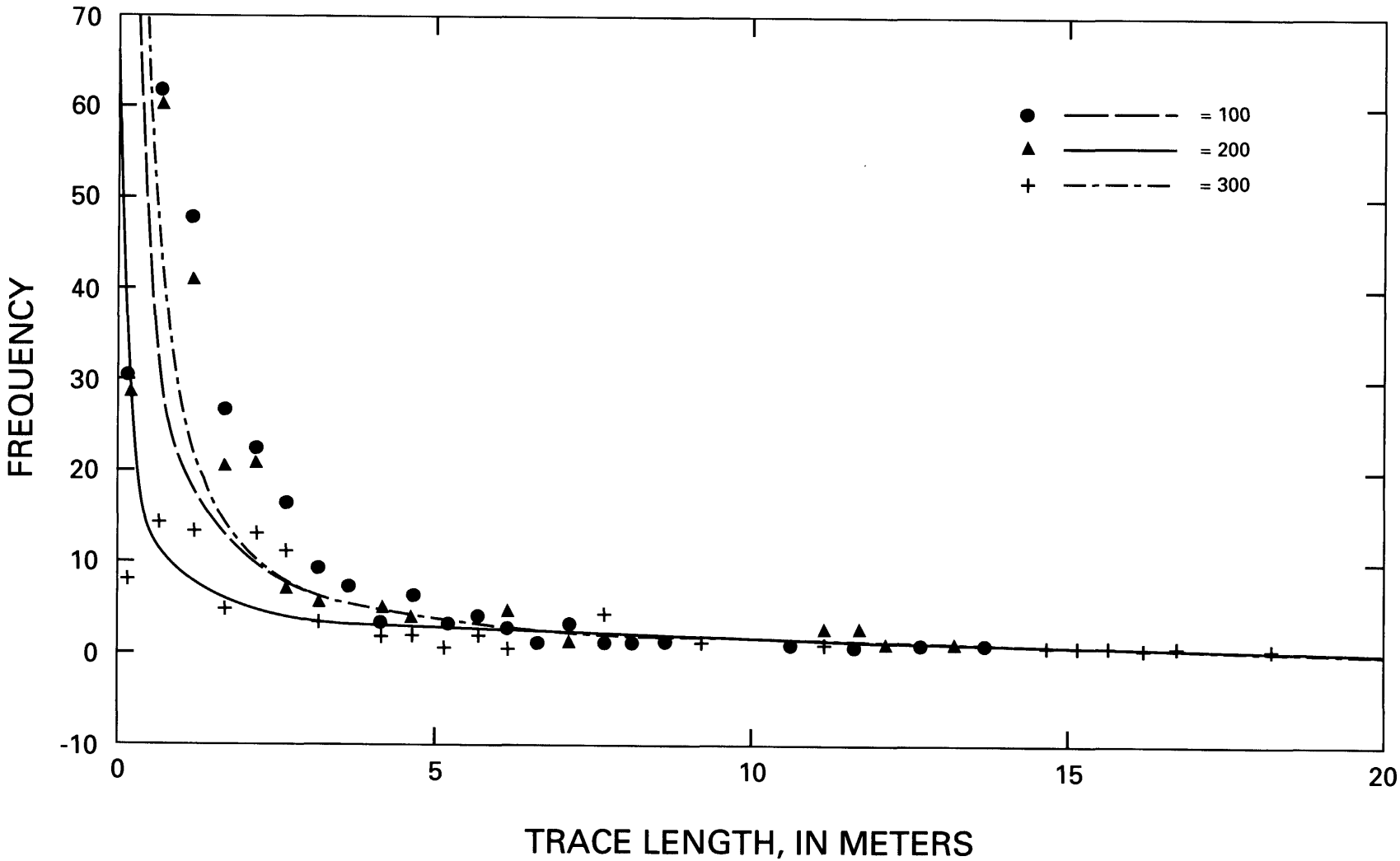

Figure 12. Frequency of fracture-trace length for pavements 100, 200, and 300.

suggest to us that extrapolation along the power-law curves to smaller and longer traces is reasonable.

We find no correlation between fracture-trace length and aperture (fig. 13). A linear correlation has been reported for completely isolated nonintersecting calcite filled fractures in two-dimensional vertical exposures (Verbeek and Grout, 1989). A correlation should not be expected for networks of intersecting open fractures, because intersecting open fractures bound blocks that rotate and slide to readjust in response to subsequent loading and unloading.

Fracture-Length Density

The density of fracturing is a parameter used in generating synthetic fracture patterns for hydrologic and geomechanical modeling. An areal fracture density can be expressed in terms of the sum of fracture-trace lengths measured on plate 1, per unit area of pavement surface. The fracture densities for pavements 100, 200, and 300 are 2.35, 1.40, and 2.35 m^{-1}, respectively.

Some areas of fracturing on the pavements are so intense that it is not possible to show each fracture on the maps. These areas are identified on plate 1 by stippling; short line segments indicate the representative azimuth of the fractures within each area. Some of these areas are bounded by one or more faults (for example, fractures F59, F105, and F109 on pavement 100). We conclude that the intense fracturing of areas bounded by faults was induced by space problems resulting from displacement along the faults. The other areas of intense fracturing are not clearly attributed to fault displacements.

Fracture Mineralization and Alteration

Minerals deposited on fracture faces can be useful for determining the relative timing of fracture genesis and for the paleohydrology of a fracture network as will be shown below.

A few of the fractures exposed on the pavements exhibit mineral coatings, some of which completely fill the aperture. Hand-lens inspection showed vapor-phase quartz crystals coating two joints on pavements 100 and 300 as shown on plate 1. The coating is pale orange-brown due to intergrowth of the quartz crystals with oxide minerals (Carlos, 1985). Visually similar coatings commonly line the surfaces of the lithophysal cavities and the tubular structures (described below) on the surfaces of the joints. If these are vapor-phase quartz crystals, then they were most likely deposited during degassing of the tuff. This would suggest that the joints formed very early, soon after emplacement of the tuff.

Another fracture filling found on the pavements is a composite material termed calcrete. Here calcrete consists of angular tuff fragments and sub-angular calcite fragments cemented by a sugary calcite matrix. A calcrete deposit can be observed bridging fracture F140 on pavement 100. The calcrete overlies a white calcite coating, which lines the fracture walls, suggesting that the calcite coating is older. Calcrete also fills depressions in all three of the pavement surfaces. We suggest that these calcrete deposits arise from dissolution and reprecipitation of windblown carbonate in evaporating rainwater pools that collect on the debris-covered bedrock surface, thus incorporating tuff fragments.

Dendritic deposits of ferro-manganese oxides and hydroxides are sporadic and can be observed on many of the fracture surfaces as well as much of the pavement surfaces and within the rock matrix. They are small spotty deposits, dark-brown to black in color. These deposits precipitate from solution and are found throughout the volcanic section at Yucca Mountain (Scott and Castellanos, 1984; Spengler and Chornack, 1984, Carlos, 1985; Zielinski and others, 1986), suggesting to us that surface water has percolated both along fractures and through the rock matrix.

In three areas of fracture intersection on pavement 200 and one on pavement 300, the tuff matrix has been altered to clay (pl. 1). These areas were excavated during clearing of the pavements and were observed to rapidly accept large quantities of water, and they are identified on plate 1 as areas of anomalously high infiltration. Their stratigraphic extent is not known, but they may be conduits for rapid movement of large quantities of water from the surface into the interior of Yucca Mountain. Alternatively, as suggested by Montazer and Wilson (1984), the fracture pathways may be limited to the welded tuff near the surface so that downward-percolating water is dispersed into deeper nonwelded units.

Fracture Connectivity

The fluid-flow properties of a fracture network are affected markedly by the degree to which the fractures are interconnected. Fractures that are not interconnected contribute little to flow through the fracture network. Connectivity can be represented by the ratios of the three types of fracture termination or interaction. Fractures may (1) terminate in the rock matrix; we term these "dead" endings. Alternatively, they may (2) cross

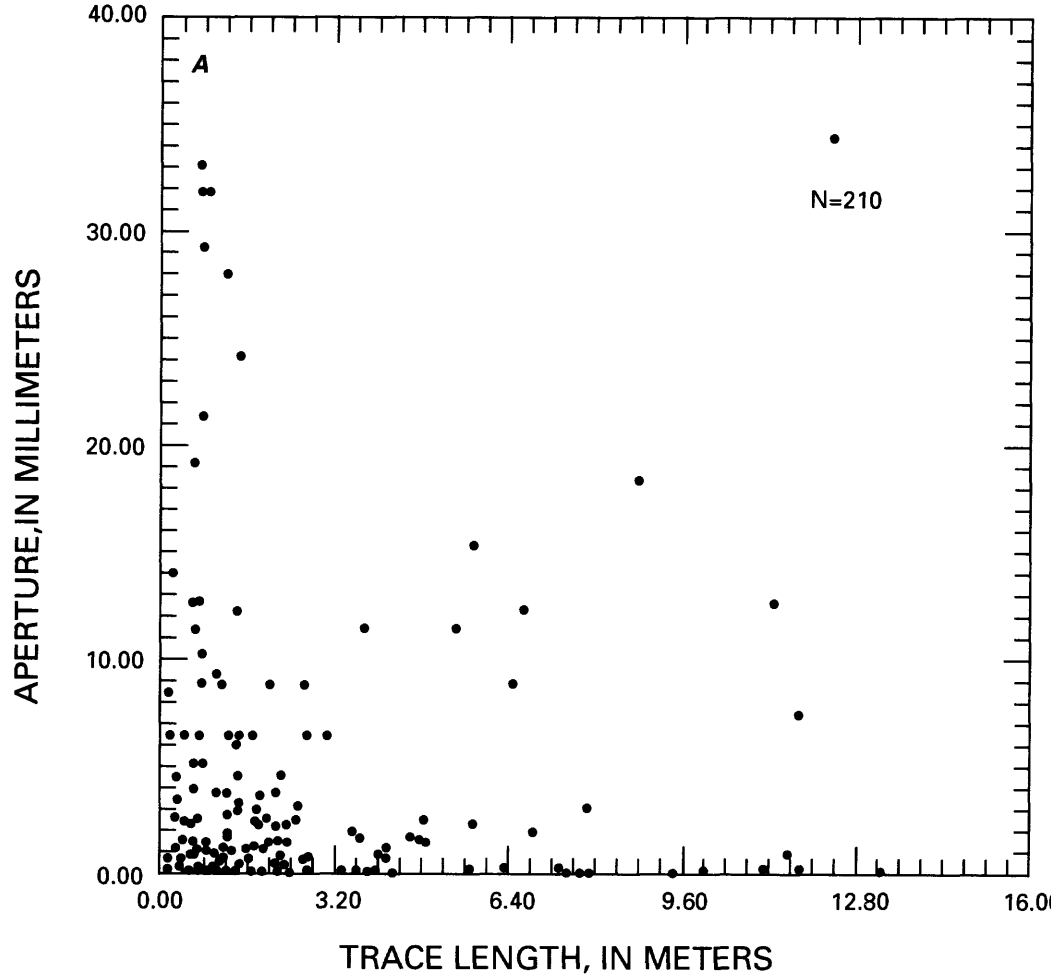

Figure 13A. Diagram of aperture as a function of trace length.
A. Pavement 100; B. Pavement 200; Pavement 300.

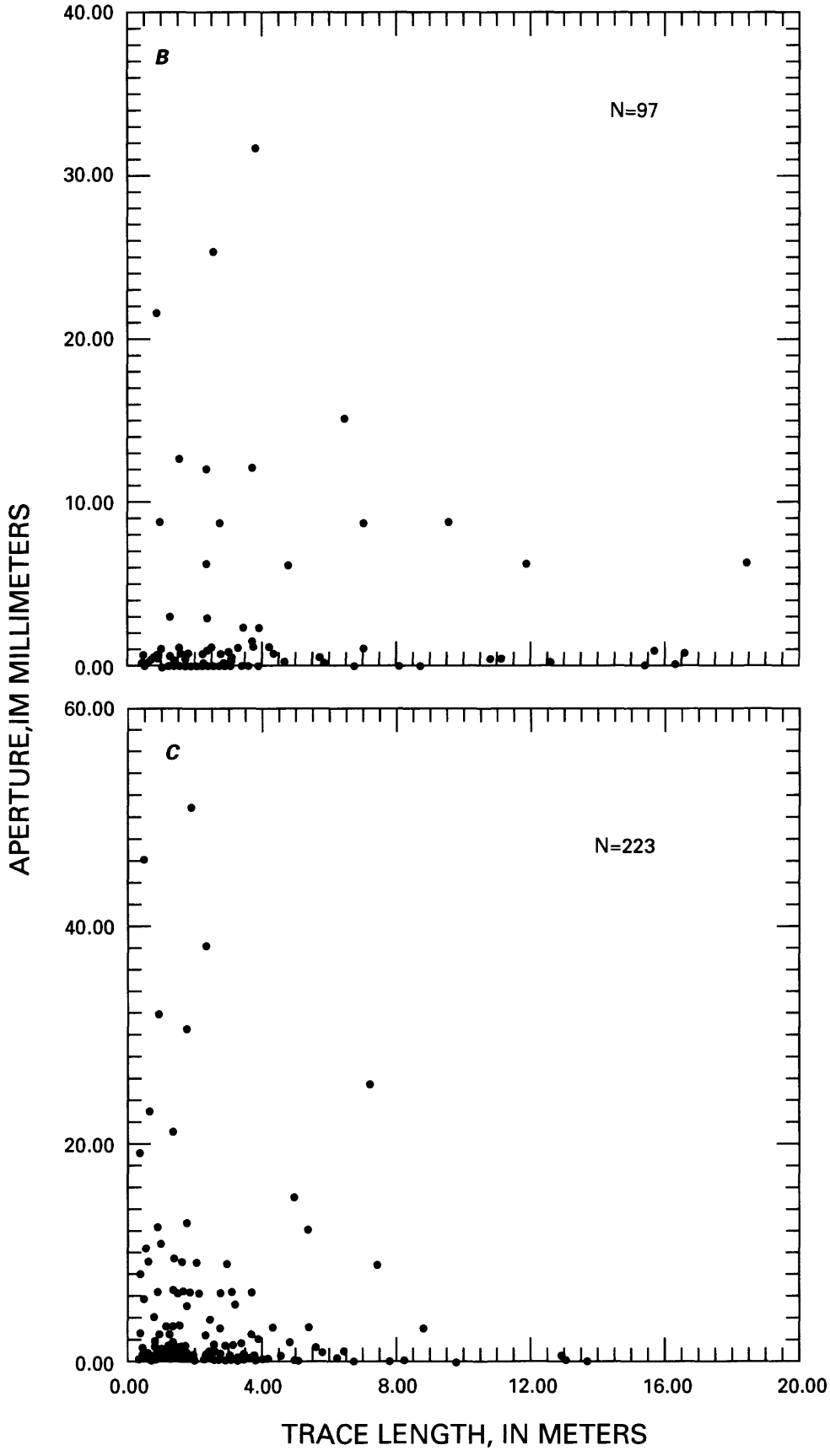

Figure 13 B and C. Diagram of aperture as a function of trace length.
A. Pavement 100; B. Pavement 200; C. Pavement 300–Continued.

or (3) abut other fractures. The percentage of fracture terminations and crossings are shown on figure 14 and listed in table 3. Dead endings and crossings are found in nearly equal proportions, but abuttings are found most frequently. The proportions for all three pavements cluster quite tightly on the ternary diagram (fig. 14).

Table 3. Proportions of Fracture Intersections and terminations

Pavement	Crossing (percent)	Abutting (percent)	Dead (percent)
100	27	40	33
200	21	51	28
300	24	50	26
100, 200, 300 combined	24	47	29

FRACTURE HISTORY

A complex pattern of fractures is exposed on the pavements (pl. 1). The pattern consists of two fracture types formed during at least three deformational events (Barton, 1984).

The first type is distinguished by open, anastomosing, matched half-tubes on opposing fracture faces (fig. 15). These fractures show only face separation without shear and are unequivocally joints. Glass spherules adjacent to the joint faces in high concentrations suggest that the joints formed, opened, and their surfaces were quenched before or during devitrification of the tuff. They are thus cooling joints.

The cooling joints make up two well-defined sets, striking 25 to 85° and 270 to 355°, both dipping perpendicular (plus or minus 6°) to foliation. Abutting of fractures of the two sets against each other suggests that they developed coevally. Both sets exhibit 3- to 5-m-wide swarms spaced 150-200 m apart. The rectangular, rather than irregular, polygonal pattern formed by the joint sets may reflect a gravitational stress anisotropy induced by a depositional slope. We suggest this on the basis of our own informal observation that mudcracks developed on a slope often form a rectangular pattern with the long sides of the rectangles parallel to the strike line of the slope, while those on a level surface form an irregular polygonal pattern.

The second fracture type is distinguished from the cooling joints by higher roughness coefficients (3 to 18) and by the absence of tubular structures on their faces. These fractures range over all azimuths and do not group into sets based on orientation or roughness. These fractures either abut against or offset the cooling joints and thus postdate them. Six of the fractures are northwest-striking, steeply dipping faults that offset cooling joints in a right-lateral sense. They are parallel to the trend of the Las Vegas Valley-Walker Lane regional shear deformation, which is also right-lateral. This suggests that the two may be related.

Tubular Structures

Open, anastomosing, matched half-tubes on opposing joint faces are present only on the cooling joint faces and are not found in the body of the rock. Tube diameters range from 0.5 to 21 mm. The tubes may exhibit one or two sets based on pitch for a given joint face and vary from face to face, ranging from 0 to 85° (fig. 16). The tube pitch is given in the appendix. Where two sets are present, the pitch of the second set is given in the remarks column of the appendix.

The anastomosing tubes isolate areas of the joint surface which we refer to as "islands". The surface of each island is slightly convex and tilted relative to neighboring islands. The tilt of the island surfaces relative to the joint surface was measured for a portion of a joint face (see fig. 17). The angle of tilt varies from 0 to 10°; the direction of tilt shows no apparent pattern. The effect of the irregular tilts is to oppose any shear motion along the joint surfaces. This may be why the cooling joints have not been subsequently reactivated in shear even though they are the oldest fractures.

The tubular structure is interpreted to be analogous to bread-crust structure on volcanic bombs (Barton and others, 1984). As stated above, the high concentration of glass spherulites adjacent to the joint faces suggests that the joints formed, opened, and their surfaces were quenched soon after emplacement of the tuff. We surmise that the tubes formed by tensile tearing in response to stretching of the quenched joint surface due to volume expansion of the tuff by exsolution and expansion of trapped volcanic gas that produced the lithophysal cavities during cooling of the tuff. The small range in the ratio of tube area to total joint face area (16 to 22 percent) for four samples, each approximately 0.8 m^2 in area, strongly supports this interpretation because it implies a locally uniform volume expansion of the tuff. Extrusion of tuff matrix into some of the tubes due to volume expansion of the tuff during exsolution and expansion of the trapped volcanic gas further supports our interpretation of the timing and mode of origin of the tubes as tears in early formed quenched joint surfaces. The lining of some of the tubes exhibits the sugary vapor phase coating of quartz observed coating the surfaces of lithophysal cavities and some of the cooling fractures. These coatings must have been deposited soon after the tuff was

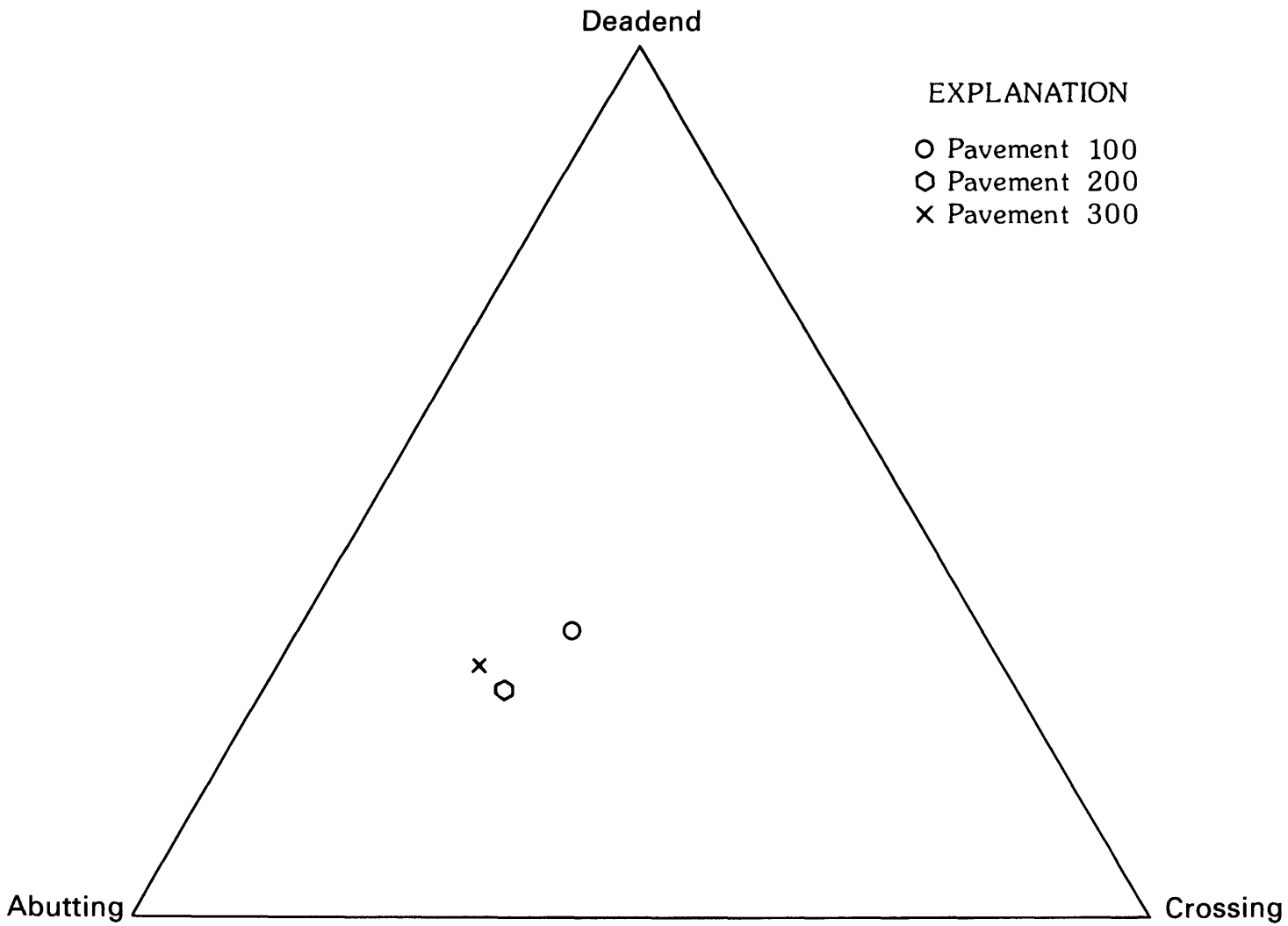

Figure 14. Ternary diagram of percentages of fracture intersections and terminations for pavements 100, 200, and 300.

Figure 15. Photograph showing tubular structures on the surface of joint J11, on pavement 300.

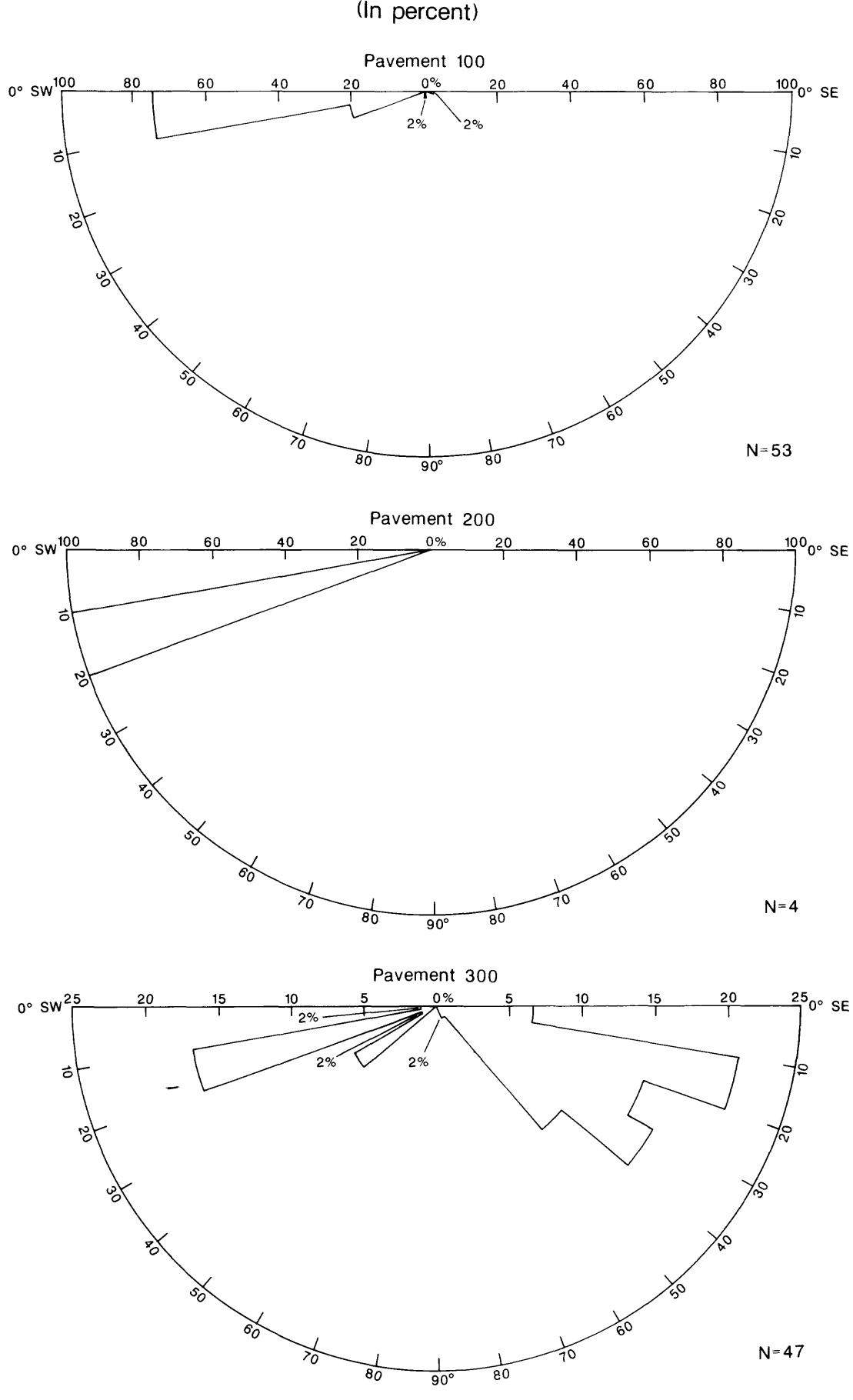

Figure 16. Diagrams of the distribution of the pitch of tubes on joints for pavements 100, 200, and 300.

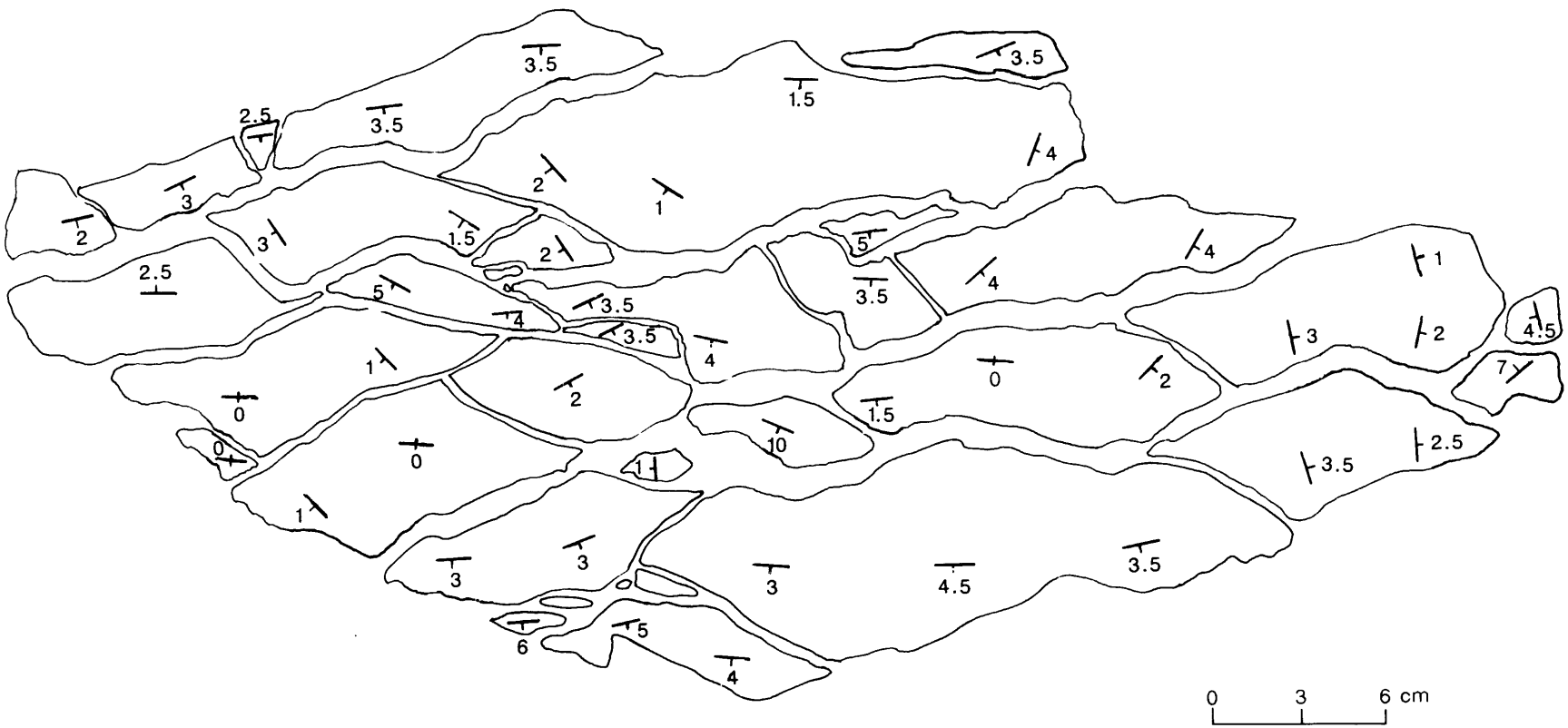

Figure 17. Plan view of a portion of a joint surface showing the direction and angle of dip for island surfaces.

emplaced, probably by the same volcanic gas that formed the lithophysal cavities. This is further evidence for the early formation of the cooling joints which must have formed prior to the tubular structures.

FRACTAL GEOMETRY OF THE FRACTURE NETWORKS

Fracture networks in rock are present over a wide range of scales, from the largest faults down to microfractures. The contribution of fracture networks to fracture-flow, mechanical stability, and physical properties of rock is not a function of the fractures at any one particular scale, but rather is the sum of the contribution of fractures at all scales. Therefore, it is useful to know the scaling function for fracture networks over a wide range of scales. The concept of fractal geometry is particularly useful for investigating scaling of complex objects if they are self-similar. Here, self-similarity means the replication of the statistical properties of geometric patterns over a range of scale. Thus, fractal patterns possess dilatation and reduction symmetry. Fractal geometry applied to two-dimensional fracture-trace networks simultaneously and jointly quantifies the spatial, trace-length, and orientation distributions (Barton and Larsen, 1985; Barton and others, 1985 and 1986; Barton and Hsieh, 1989).

We have greatly improved our technique for determining the fractal properties of fracture-networks. The use of computers permits us to easily sample a greater number of intermediate scales than we could in our earlier papers and thereby to more finely sample the fractal behavior and more accurately determine the fractal dimension of the networks.

Our investigations of the box method also indicate that the range of box sizes for sampling the fractal properties of a fracture network is limited by the network itself. The smallest box size should be no smaller than the shortest fracture in the network, while the largest box size should be smaller than the size at which all the boxes are occupied. The fractal dimensions for pavements 100, 200, and 300 were reported previously as ranging from 1.12-1.16 (Barton and Larsen, 1985). These values were calculated for cell sizes at or below the shortest fracture length and thus are unrepresentative of the fracture network. The same maps were reanalyzed in Barton and Hsieh (1989) including box sizes that were too large; the fractal dimensions reported ranged from 1.6-1.7.

We use a variation of the box method which we term the box-flex method for fractal analysis, developed by the senior author. In this method, grids of various-sized square cells are placed successively over the maps, and the number of cells intersected by fracture traces counted. The outer boundaries of the grid are permitted to expand (or flex) so that the box size can be changed by very small increments. For each of the plots shown on figure 18, fifty different box sizes were used, which produces a fractal dimension with an accuracy of plus or minus 0.05.

The fractal distribution of lines on a map is

$$Nr^D = 1 \qquad (2)$$

or equivalently

$$D = \log N / \log(1/r) \qquad (3)$$

where N is the least number of cells containing portions of one or more fracture traces, r is the length of the side of each cell, and D is the fractal dimension. On figure 18, the log (1/r) is plotted versus log (N) for each element size. The fractal dimension D is the slope of a straight line fitted to the points. The fractal dimensions of all three networks lie between 1 (the dimension of a straight line) and 2 (the dimension of a filled plane). Pavement 100 has a fractal dimension of 1.5; pavement 200, 1.4; and pavement 300, 1.5, all determined to confidence levels of 0.99.

Because the points can be fitted by smooth lines (either straight or curved), the networks can be said to be fractal over the range of r sampled. Because these lines are straight (not curved), the networks can also be said to be scale independent over the same range. The fractal dimension is a quantitative measure of scaling. The fractal dimension for a fourth pavement (pavement 100), mapped at 1:50 in the orange-brick unit of the Topopah Spring Member of the Miocene Paintbrush Tuff at Yucca Mountain is 1.7 (figure 18) which is significantly higher than the dimensions 1.4-1.5 determined for the three pavements mapped at 1:50 in the upper-lithophysal unit of the Tiva Canyon Member. The fractal dimension for the network of faults mapped at 1:12,000 by Scott and Bonk (1984) is 1.5 (figure 18), which is equal to the average of the range of the dimensions for the four pavements included in this study. This suggests that the fractal properties of fracture networks are scale independent over a broad range of scales at Yucca Mountain and are independent of the mode of origin of the fractures as faults or joints. If fractal analyses of future fracture maps at different scales and locations on Yucca Mountain have the same range as the results presented above, then it will be acceptable to map fractures at one scale and extrapolate the spatial and statistical geometric properties to larger and smaller scales.

Once the fractal dimension of a pattern or object in nature is determined, it is possible to model that pattern or object from a single generator. A generator is

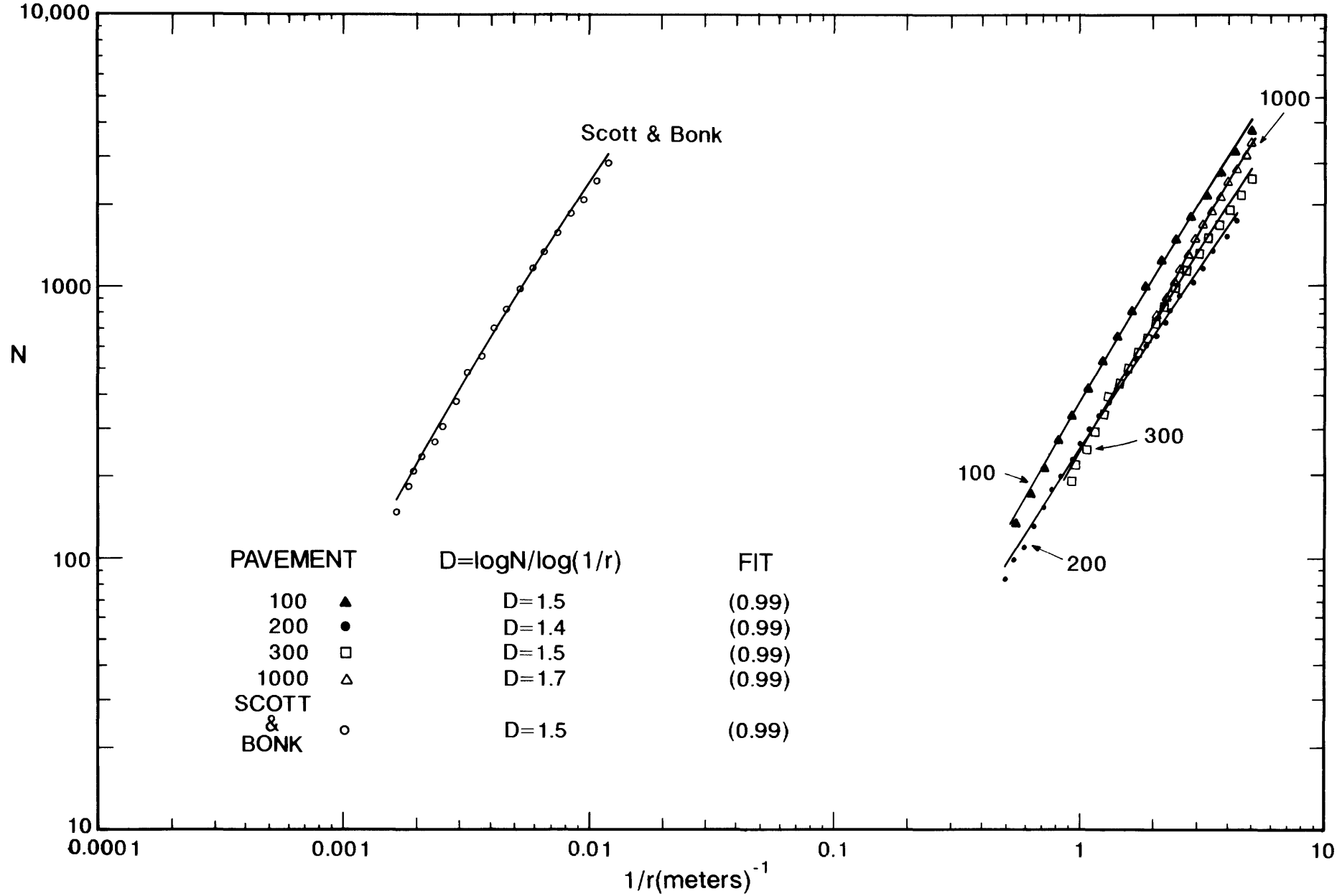

Figure 18. Fractal plot of fracture networks mapped on pavements 100, 200, and 300, and for the fault network mapped by Scott and Bonk (1985).

the fundamental building block from which a fractal pattern or object is generated by iterative replacement of each piece of the generator by a reduced version of the generator. The task of deducing a generator for a particular fractal pattern observed in nature is not easy. One approach is to guess the generator as was done by King (1983) for the map pattern of the traces of subsidiary faults in the immediate vicinity of large-scale fault bends. The box method has an intrinsic upper limit of 2.0 for the fractal dimension of patterns of lines lying in a plane. Nonoverlapping fractal generators that lie in a plane also have an upper limit of 2, while overlapping fractal generators lying in a plane can exceed 2.0. For ten pavements we have studied, we have not found fractal dimensions of fracture traces to exceed 1.7, and we conclude that their generators are not space filling. In order to simulate fault patterns, King (1983) proposed a three dimensional space-filling generator, but assumed that it was never fully formed. In a two-dimensional section, the equivalent is a fractal dust with a dimension of 1.0 which falls below the values we have measured for the pavements which are also two dimensional. We commonly observe crosscutting fractures on our maps which suggest that a proper generator for modeling fracture trace patterns should be overlapping. The generator proposed by King (1983) was for shear faults that did not overlap and therefore is not appropriate for the patterns of crossing fractures. We have been unsuccessful at guessing a generator for modeling our fracture-trace maps. A most promising method for deducing a fractal generator is the iterated function systems approach being developed by Barnsley and Demko (1985) which systematically deduces a fractal generator for a given fractal object.

PATTERN OF DEVELOPMENT OF FRACTURE NETWORKS

Fracture networks evolve from initially ordered to increasingly disordered patterns. Fracture networks become more complex with time as new fracture generations are added to those that already exist. Generations of fractures form during discrete episodes, each of which records a discrete element of the tectonic history. Most episodes of fracturing are not accompanied by major tectonic deformations such as folding and faulting. If we can determine that the fractures in a network formed in extension, then we can determine the relative ages on the basis of abutting relations—younger fractures abut older ones. We have thus analyzed joint patterns mapped on pavements 100, 200, and 300.

Analysis of fracture characteristics from one generation to the next reveals the following pattern of fracture-network development. In general, the first-generation fractures (i.e. the cooling fractures) are long, subparallel, and connectivity is poor. Second-generation fractures are shorter and abut the first-generation fractures, generally at high angles, to form large, polygonal blocks; connectivity is improved. Fractures of subsequent younger generations are generally shorter, more diversely oriented, and increase connectivity greatly. The younger fractures define small, irregular polygonal blocks bounded by the older fractures. The pattern of evolution should begin again when mineral infillings mechanically heal previous fracture generations. This predicts that one or more stages of infilling are required to permit highly ordered fracture patterns composed of more than one or two generations of fractures. Highly ordered fracture patterns are not observed in the stratigraphic section at Yucca Mountain, probably because there has been little healing of fractures by mineral infilling.

The spatial distribution of fractures and connectivity within the network evolve as fractures are sequentially added to the network. The fractal dimension of patterns of fracture traces, ranges from about 1 for early stages of network development to 1.7 for mature networks. Connectivity within the network is low during initial stages of development and increases as more fractures are added.

During evolution of the network, larger blocks are preferentially broken by subsequent fracturing; this process reduces the range of block sizes. The opposite has been reported for comminution by grinding which produces a fractal distribution of particle sizes over six orders of magnitude in scale (Sammis and Biegel, 1989; Turcotte, 1986); this suggests that the physics of grinding involves more than fracturing.

Younger fractures apparently formed in response to local stress conditions within the blocks in which they formed, and thus are less useful than first generation fractures for determination of regional paleostress orientations. The evolution of fracture patterns described above is the basis for our computer generation of synthetic fracture networks (Barton and others, 1987).

DISCUSSION

A method for characterizing fractures for fluid-flow, geomechanical, and paleostress modeling has been developed and applied at three localities in the vicinity of USW G-4 at Yucca Mountain. The basis for the method is clearing pavement exposures and making a map of fracture traces and intersections. This method provides for optimal sampling of the characteristics of both individual fractures and fracture networks. The standard geologic methods for characterizing fractures use outcrops, boreholes and cores, and aerial photo-

graphs. These methods, alone or in combination, rarely permit measurement of the variety of fracture data with the accuracy that the pavement method permits. The pavement method is feasible wherever debris cover can be removed.

Outcrops permit measure of orientation, roughness, mineralization, aperture, and tectonic features. But, normally there is little choice in where to measure these characteristics because only a very small portion of each fracture is exposed. Where outcrop size is limited, usually it is not possible to determine trace length, spatial distribution of traces and their intersections, connectivity, or the sizes, shapes, and geometries of blocks bounded by fractures. These are characteristics of the network that are necessary for hydrologic, geomechanical, and paleostress modeling.

Boreholes and cores together can provide orientation, roughness, mineralization, aperture, and tectonic features. But, there is very little choice of where to measure these characteristics because only a very small portion of the fracture is recovered or exposed in the borehole wall. It is impossible to determine trace length, spatial distribution of traces and intersections, connectivity, most abutting relations, or the size, shape, and spatial distribution of blocks bounded by fractures. The primary limitation of boreholes and cores is that they are a one-dimensional sampling of a three-dimensional fracture network. Moreover, in flat-lying strata, boreholes and cores are normally subparallel to the dip of most of the fractures. They provide a limited and biased sampling of fractures that cannot be corrected by statistical analysis.

Aerial photographs have proven to be the poorest method at Yucca Mountain. At best they could provide trend (but not dip) and spatial patterns and densities. At Yucca Mountain they cannot even provide these characteristics; linear features on the photographs have been shown not to correspond to fractures on the ground (Throckmorton, 1987).

The pavement method is not perfect, but it does permit a more accurate and complete sampling of the individual and network characteristics of fractures. Pavements are only a two-dimensional sampling of a three-dimensional fracture network. Optimally, a comprehensive study will include pavements in three perpendicular planes.

The size of pavements is necessarily limited by time, funding, and environmental constraints. The size of all of these pavements falls short of revealing a characteristic, representative elementary area of the fracture pattern. A larger pavement, 1720 m^2 in area in the same upper lithophysal unit of the Tiva Canyon member exposed on top of Busted Butte, 9 km to the south and mapped subsequent to this study, does not reveal a representative elementary area with a characteristic length scale (Bear, 1972) for the fracture pattern, implying either that prohibitively large pavements are required or that there is no representative elementary area for the fracture pattern in this unit. The fractal behavior of fracture and fault-trace patterns discussed above strongly suggests that they are self-similar and scaling over a broad range of scales at Yucca Mountain. Therefore, fractal geometry of the fracture-trace patterns is useful for extrapolating scaling and statistical geometric properties both upward and downward in scale from the necessarily limited scale of the pavements.

Pavements at the ground surface are subject to weathering and stress release. Underground, exposures are subject to the stress redistribution around all underground surfaces. Nevertheless, we conclude that the pavement method is at present the best method for characterizing fractures and fracture networks for hydrologic, geomechanical, and paleostress modeling.

CONCLUSIONS

A complex network of fractures was exposed on three 214- to 260-m^2 pavements cleared of debris in the upper lithophysal unit of the Tiva Canyon Member of the Miocene Paintbrush Tuff (pl. 1).

The network consists of two fracture types. The first type is distinguished by low surface roughness coefficients (95 percent are 1 to 4) and by open, anastomosing, matched half-tubes on opposing fracture faces. These fractures show only face separation without shear and are termed joints. Glass spherulites adjacent to joint faces suggest that the joints formed, opened, and their surfaces were quenched before or during devitrification of the tuff, and are thus cooling joints. The tubular structure is interpreted to be analogous to bread-crust structure on volcanic bombs. The cooling joints make up two well-defined sets striking 25-85° and 270-355°, both dipping perpendicular (plus or minus 6°) to foliation. Abutting of the two sets against each other suggests that they developed coevally. Both sets exhibit 3- to 5-m-wide swarms spaced 150-200 m apart. The second fracture type is distinguished by higher surface roughness coefficients (98 percent are 4 to 18) and by the absence of tubular structures on their faces. Six of these fractures have demonstrable right-lateral shear offset and are thus faults. For most of the second type of fractures, it was not possible to determine whether there was any shear displacement, and these are referred to as fractures. The fractures abut against and the faults offset the cooling joints, thus, both postdate the joints. Unlike the cooling joints,

these fractures do not form sets based on orientation or surface roughness.

The surface-roughness coefficients for the fractures and faults combined are normally distributed with peaks at RC = 10. The RC for the cooling joints is also normally distributed with peaks at RC = 2. Aperture frequency and trace-length frequency are best fit by power laws.

The networks of fractures, joints, and faults mapped on the three pavements exposed in the upper lithophysal unit of the Tiva Canyon member of the Paintbrush tuff are shown to be fractal, and the fractal dimensions (D) are 1.5, 1.4, 1.5.

ACKNOWLEDGMENTS

We gratefully acknowledge Kurt Sternlof, Mark Yallom, David Verardo, and Robert Scott of theU.S. Geological Survey, and Kirstin Johnson, Sandra Waddell, and Michael Chornack of Fenix & Scisson, Inc. for their assistance in clearing the pavements. Work was performed under Interagency Agreement DE-AI08-78ET44802 with the U.S. Department of Energy. Analysis and interpretation of the data presented in this paper have been limited by a stop-work order that prevented the collection of additional data and the re-examination of the pavement sites.

REFERENCES CITED

Barnsley, M.F., and Demko, S., 1985, Iterated function systems and the global construction of fractals: Proceedings of the Royal Society of London, A399, p. 243-275. (NNA.920814.0107)

Barton, C.C., 1984, Tectonic significance of fractures in welded tuff, Yucca Mountain, southwest Nevada (abs.): Geologic Society of America, Abstracts with Programs, v. 16, no. 6, p. 438. (HQS.880517.1057)

Barton, C.C., and Hsieh, P.A., 1989, Physical and hydrologic flow properties of fractures: Field trip guidebook T385: International Geologic Congress, 28th, Washington, D.C., American Geophysical Union, 36 p. (HQX.890818.0028)

Barton, C.C., Howard, T.M., and Larsen, Eric, 1984, Tubular structures on the faces of cooling joints—A new volcanic feature (abs.): Eos, Transactions of the American Geophysical Union, v. 65, no. 45, p. 1148. (NNA.920814.0109)

Barton, C.C., and Larsen, Eric, 1985, Fractal geometry of two-dimensional fracture networks at Yucca Mountain, southwest Nevada, *in* Stephannson, Ove, ed., Fundamentals of rock joints: Proceedings of the International Symposium on Fundamentals of Rock Joints, Bjorkliden, Sweden, p. 77-84. (NNA.920727.0028)

Barton, C.C., Larsen, Eric, and Baechle, P.E., 1985, Fractal geometry of two-dimensional sections through fracture networks at Yucca Mountain, southwestern Nevada (abs.): Eos, Transactions of the American Geophysical Union, v. 66, no. 46, p. 1089. (HQS.880517.3020)

Barton, C.C., Gott, C.B., and Montgomery, J.R., 1986, Fractal scaling of fracture and fault maps at Yucca Mountain, southern Nevada (abs.): Eos (Transactions of the American Geophysical Union), v. 67, no. 44, p. 870. (HQS.880517.3021)

Barton, C.C., Page, W.R., and Larsen, Eric, 1986, Pattern of development of fracture networks: Geologic Society of America, Abstracts with Programs, v. 18, no. 6, p. 536. (NNA.920616.0002)

Barton, C.C., Schutter, T.A., Page, W.R., and Samuel, J.K., 1987, Computer generation of fracture networks for hydrologic-flow modeling: Eos (Transactions of the American Geophysical Union), vol. 68, no. 44, p. 1295. (NNA.920814.0108)

Barton, N.R., and Choubey, V., 1977, The shear strength of rock joints in theory and practice: Rock Mechanics, v. 10, p. 1-54. (HQS.880517.2610)

Bear, Jacob, 1972, Dynamics of fluids in a porous media: American Elsevier, New York, 746 p. (NNA.890713.0163)

Brown, S.R., and Scholz, C.H., 1985, Closure of random elastic surfaces in contact: Journal of Geophysical Research, v. 90, no. B7, p. 5531-5545. (NNA.900403.0013)

Byers, F.M., Jr., Carr, W.J., Orkild, P.P., Quinlivan, W.D., and Sargent, K.A., 1976, Volcanic suites and related cauldrons of Timber Mountain-Oasis Valley caldera complex, Southern Nevada: U.S. Geological Survey Professional Paper 919, 70 p. (NNA.870406.0239)

Carlos, B.A., 1985, Minerals in fractures in the unsaturated zone from drill core USW G-4, Yucca Mountain, Nye County, Nevada: Los Alamos National Laboratory Report LA-10415-MS, 55 p. (HQS.880517.1112)

Cook, N.G.W., 1992, Natural joints in rock; mechanical, hydraulic and seismic behavior and properties under normal stress: Jaeger Memorial Lecture, presented at the 29th U.S. Symposium on Rock Mechanics, 1988, International Journal of Rock Mechanics and Mining Sciences and Geomechanics Abstracts, v. 29, no. 3, p. 198-223. (NNA.930602.0002)

Dershowitz, William, Geier, J., Axelsson, C.L., 1991, Application of discrete feature analysis to repository characterization: High Level Radioactive Waste Management and Proceedings of the Second Annual Conference, Las Vegas, Nevada, April 28-May 3, 1991, American Society of Civil Engineers, New York, p. 272-278. (NNA.920917.0056)

Goodman, R.E., and Shi, G.H., 1985, Block theory and its application to rock engineering: Englewood, N.J., Prentice-Hall, 388 p. (NNA.890522.0212)

Haimson, B.C., Lacomb, J., Jones, A.H., and Green, S.J., 1974, Deep stress measurement in tuff at the Nevada Test Site: Advances in Rock Mechanics, v. IIa, National Academy of Sciences, Washington D.C., p. 557-561. (NNA.920917.0057)

King, G.C.P., 1983, The accommodation of large strains in the upper lithosphere of the earth and other solids by self-similar fault systems: the geometric origin of b-value: Pure and Applied Geophysics, V. 121, no. 5/6, p. 761-816. (NNA.920616.0003)

Kulander, B.R., Barton, C.C., and Dean, S.L., 1979, Applications of fractography to core and outcrop investigations: U.S. Department of Energy Report METC/SP-79/3, 179 p. (NNA.920727.0030)

La Pointe, P.R., and Hudson, J.A., 1985, Characterization and interpretation of rock mass joint patterns: Geological Society of America Special Paper 199, 37. p. (NNA.920616.0004)

Lemos, J.V., Hart, R.D., and Cundall, P.A., 1985, A generalized distinct element program for modelling jointed rock mass, in Stephannson, Ove, ed., Fundamentals of rock joints: Proceedings of the International Symposium on Fundamentals of Rock Joints, Bjorkliden, Sweden, p. 335-343 (NNA.920727.0029)

Long, J.C.S., 1983, Investigation of equivalent porous medium permeability in networks of discontinuous fractures: Lawrence Berkeley National Laboratory Report LBL-16259, 277 p. (NNA.921019.0194)

Long, J.C.S., Endo, H.K., Karasaki, Kenzi, Pyrak, Laura, MacLean, Peggy, and Witherspoon, P.A., 1985, Hydrologic behavior of fracture networks, *in* Hydrology of rocks of low permeability: International Association of Hydrogeologists, Memoirs, v. 17, part 2, Proceedings, (published by a committee of U.S.A. members of the International Association of Hydrogeologists), p. 449-462. (NNA.920814.0110)

Mandelbrot, B.B., 1982, The fractal geometry of nature: San Francisco, Calif., W.H. Freeman and Co., 460 p. (NNA.900123.0062)

Montazer, Parviz, and Wilson, W.E., 1984, Conceptual hydrologic model of flow in the unsaturated zone, Yucca Mountain, Nevada: U.S. Geological Survey Water Resources Investigations Report 84-4345, 55 p. (NNA.870519.0109)

Olson, Jon, and Pollard, D.D., 1989, Inferring paleostress from natural fracture patterns: a new method: Geology, v. 17, no. 4, p. 345-348. (NNA.920814.0106)

Robinson, P.C., 1984, Connectivity, flow and transport in network models of fractured media: Ph.D. dissertation, Oxford University, Oxford, England, 154 p. (NNA.930602.0008)

Rogers, A.M., Harmsen, S.C., Carr, W.J., and Spence, W., 1983, Southern Great Basin seismological data report for 1981 and preliminary data analysis: U.S. Geological Survey Open-File Report 83-669, 243 p. (NNA.870427.0085)

Sammis, C.G., and Biegel, R.L., 1989, Fractals, fault-gouge, and friction: Pure and Applied Geophysics, vol. 131, nos. 1/2, p. 255-272. (NNA.910215.0266)

Science Applications International, 1988, Yucca Mountain Project Site Atlas, Volume 1: U.S. Department of Energy, YMP/88-21, Geologic Pavements, Section 4.1.10, p. 1-7. (NNA.920917.0063)

Scott, R.B., 1984, Internal deformation of blocks bounded by Basin-and-Range-style faults (abs.): Geological Society of America, Abstracts with Programs, v. 16, no. 6, p. 649. (HQS.880517.1441)

Scott, R.B., 1986, Extensional tectonics at Yucca Mountain, southern Nevada (abs.): Geological Society of America, Abstracts with Programs, v. 18, no. 5, p. 411. (HQS.880517.1442)

Scott, R.B., Bath, G.D., Flanigan, V.J., Hoover, D.B., Rosenbaum, J.G., and Spengler, R.W., 1984, Geological and geophysical evidence of structures in northwest-trending washes, Yucca Mountain, southern Nevada, and their possible significance to a nuclear waste repository in the unsaturated zone: U.S. Geological Survey Open-File Report 84-567, 23 p. (NNA.870519.0101)

Scott, R.B., and Bonk, Jerry, 1984, Preliminary geologic map of Yucca Mountain, Nye County, Nevada, with geologic sections: U.S. Geological Survey Open-File Report 84-494, scale 1:12,000. (HQS.880517.1443)

Scott, R.B., and Castellanos, Mayra, 1984, Stratigraphy and structural relations of volcanic rocks in drill holes USW GU-3 and USW G-3, Yucca Mountain, Nye County, Nevada: U.S. Geological Survey Open-File Report 84-491, 121 p. (NNA.890804.0017)

Segall, Paul, and Pollard, D.D., 1983a, Joint formation in granitic rock of the Sierra Nevada: Geologic Society of America Bulletin, v. 94, p. 563-575. (NNA.920616.0005)

Segall, Paul, and Pollard, D.D., 1983b, Nucleation and growth of strike slip faults in granite: Journal of Geophysical Research, v. 88, no. B1, p. 555-568. (NNA.920616.0006)

Spengler, R.W., and Chornack, M.P., 1984, Stratigraphic and structural characteristics of volcanic rocks in core hole USW G-4, Yucca Mountain, Nye County, Nevada, with a section on geophysical logs by D.C. Muller and J.E. Kibler: U.S. Geological Survey Open-File Report 84-789, 77 p. (NNA.890804.0012)

Springer, J.E., Thorpe, R.K., and McKague, H.L., 1984, Borehole elongation and its relation to tectonic stress at the Nevada Test Site: Lawrence Livermore National

Laboratory Report UCRL-53528, 43 p. (HQS.880519.1711)
Stock, J.M., Healy, J.H., Hickman, S.H., and Zoback, M.D., 1985, Hydraulic fracturing stress measurements at Yucca Mountain, Nevada, and relationship to the regional stress field: Journal of Geophysical Research, v. 90, no. B10, p. 8691-8706. (HQS.880517.1509)
Throckmorton, C.K., 1987, Photogeologic study of linear features near a potential nuclear-waste repository site at Yucca Mountain, southern Nye county, Nevada: U.S. Geological Survey Open-File Report 87-409, 54 p. (HQX.880125.0018)
Turcotte, D.L., 1986, Fractals and fragmentation: Journal of Geophysical Research, vol. 91, no. B2, p. 1921-1926. (NNA.920605.0070)
U.S. Geological Survey, 1984, A summary of geologic studies through January 1, 1983, of a potential high-level radioactive waste repository site at Yucca Mountain, southern Nye County, Nevada: U.S. Geological Survey Open-File Report 84-792, 103 p. (NNA.891009.0304)
Verbeek, E.R., and Grout, M.A., 1989, Variation in fracture network characteristics among coexisting lithologies of Mesaverde group, DeBeque Canyon, western Colorado: American Association of Petroleum Geologists, Bulletin, vol. 73, no. 9, p. 1177. (NNA.920814.0105)
Wu, S.S.C., 1985, Topographic maps of Yucca Mountain area, Nye County Nevada: U.S. Geological Survey Open-File Report 85-620, scale 1:5000. (HQS.880517.1929)
Zielinski, R.A., Bush, C.A., Spengler, R.W., and Szabo, B.J., 1986, Rock-water interaction in ash-flow tuffs (Yucca Mountain, Nevada, U.S.A.)-the record from uranium studies: Uranium, v. 2, p. 361-386. (NNA.900820.0268)

APPENDIX

APPENDIX

Compilation of fracture number, azimuth (AZI), dip, dip direction (DIP DIR), aperture, length, roughness coefficient (R.C.), and tube pitch for pavements 100, 200, and 300.

Symbols

H = Healed fracture or joint

O = Open fracture or joint, no aperture

PH = Partially healed fracture or joint

SW = Fracture or joint swarm

\- = Value unobtainable

-- = Feature not present

APPENDIX. Pavement 100, 200, and 300

Fracture number	AZI	DIP	DIP DIR	Aperture (mm)	Length (m)	R.C.	Pitch	Remarks
				PAVEMENT 100				
J1	230	66	320	1.02	1.30	-	6SW	
J2	229	80	319	6.40	1.50	3	0	
J3.1	223	83	313	8.90	2.10	4	85SW	
J3.2	221	72	311	2.40	5.80	3	6SW	
J4	226	73	316	0.05	1.70	4	6SW	
J5	227	84	317	0.05	3.90	3	2SW	PH
J6	214	75	304	34.30	12.40	1	8SW	
J7	230	73	320	1.27	1.70	4	-	
J8	234	74	324	0.05	4.30	3	-	PH
J9	225	74	315	0.64	2.70	2	8SW	
J10	227	72	317	0.05	8.00	2	10SW	PH
J11	238	63	328	1.27	1.80	-	10SW	PH
J12	235	68	325	5.10	0.80	-	-	
J13	232	79	322	0.31	7.40	1	5SW	
J14A	211	70	301	1.20	2.00	3	-	
J14B	224	71	314	0.81	4.10	2	3SW	
J15	232	81	322	0.31	2.50	3	7SW	
J16.1	226	70	316	12.70	11.30	4	14SW	
J16.2	225	83	315	0.70	0.20	-	-	
J17.1	229	80	319	0.31	11.80	1	12SW	
J17.2	223	79	313	-	0.40	2	6SW	O
J17.3	220	-	310	-	0.60	-	-	
J17.4	230	82	320	0.05	2.30	2	9SW	
J18.1	227	83	317	1.02	11.60	1	7SW	
J18.2	234	77	324	0.61	0.50	-	-	
J18.3	235	85	325	3.50	0.40	3	-	
J18.4	241	81	331	1.70	0.50	-	-	PH
J19	235	89	325	0.05	4.00	3	7SW	
J20	228	85	318	0.05	10.10	3	13SW	PH
J21	227	84	317	0.26	11.20	2	3SW	
J22	231	86	321	0.38	6.40	2	-	
J23	262	86	352	0.05	9.50	1	11SW	PH
J24	228	83	318	0.13	4.30	1	10SW	
J25	221	85	311	0.05	0.80	2	-	
J26	316	88	46	0.76	4.20	1	13SE	PH
J27	319	82	49	-	3.20	3	3SE	O
J28	227	75	317	0.13	2.40	2	-	PH
J29	233	65	323	0.05	1.50	4	6SW	PH
J30	232	68	322	0.05	0.50	4	4SW	PH
J31.1	230	76	320	0.05	0.80	1	10SW	
J31.2	239	-	329	-	0.50	-	-	
J31.3	239	83	329	2.40	0.60	2	4SW	PH

APPENDIX. Pavement 100, 200, and 300 --Continued

Fracture number	AZI	DIP	DIP DIR	Aperture (mm)	Length (m)	R.C.	Pitch	Remarks
			PAVEMENT 100--Continued					
J31.4	227	78	317	1.14	4.20	1	9SW	
J31.5	230	76	320	3.00	1.50	3	5SW	
J31.6	223	80	313	-	1.00	2	16SW	O
J32.1	230	80	320	0.76	1.10	2	6SW	
J32.2	226	80	316	0.56	1.70	2	-	
J33	222	74	312	0.05	0.70	1	-	
J34.1	233	82	323	0.04	1.20	1	11SW	
J34.2	228	87	318	1.78	3.70	1	-	
J34.3	223	77	313	0.71	1.70	2	-	
J34.4	225	89	315	6.00	1.45	-	2SW	
J35.1	49	90	139	1.91	3.60	2	6SW	
J35.2	233	84	323	1.47	2.10	1	9SW	
J36.1	227	89	317	2.54	4.90	1	6SW	
J36.2	230	88	320	2.28	2.20	2	5SW	
J37	226	82	316	0.64	0.40	2	3SW	
J38	228	83	318	31.80	0.80	4	4SW	
J39	221	83	311	1.65	0.60	4	3SW	
J40.1	228	84	318	0.64	2.80	2	5SW	
J40.2	225	84	315	1.57	2.30	2	10SW	
J41.1	231	83	321	0.64	2.30	1	10SW	
J41.2	228	86	318	1.47	2.40	3	7SW	
J42	311	81	41	14.00	0.30	3	-	
J43.1	232	80	322	-	0.50	1	10SW	O
J43.2	227	85	317	0.05	2.40	1	13SW	
J43.3	226	87	316	0.30	2.50	2	11SW	
J44	287	87	17	0.56	0.50	-	-	
J45.1	225	81	315	1.27	1.30	4	12SW	
J45.2	224	83	314	0.43	1.70	-	-	
J45.3	225	87	315	-	0.85	1	20SW	O
J46	315	80	45	0.05	0.70	1	4SE	
J47.1	225	82	315	1.91	1.30	2	8SW	
J47.2	220	74	310	-	0.80	2	3SW	O
F1	65	88	155	0.05	0.60	8	--	
F2	235	75	325	31.80	1.00	10	--	
F3	133	69	223	3.20	2.60	5	--	
F4	316	82	46	2.70	0.30	8	--	
F5	286	87	16	2.30	1.90		--	
F6	6	79	96	0.90	0.80	-	--	
F7	225	80	315	0.64	1.30	11	--	
F8	255	85	345	0.51	1.70	12	--	
F9	226	76	316	3.80	2.20	8	--	
F10	230	66	320	-	2.00	6	--	O
F11	161	54	251	3.10	1.80	8	--	
F12	266	46	356	19.10	0.70	9	--	

APPENDIX. Pavement 100, 200, and 300 --Continued

Fracture number	AZI	DIP	DIP DIR	Aperture (mm)	Length (m)	R.C.	Pitch	Remarks
			PAVEMENT 100--Continued					
F13	145	85	235	4.60	1.50	12	--	
F14	270	66	0	1.52	0.70	12	--	
F15	9	68	99	7.60	11.80	5	--	
F16	210	86	300	0.04	1.50	12	--	
F17	29	83	119	0.15	1.90	12	--	
F18	46	85	136	0.30	0.50	8	--	
F19	43	73	133	2.50	0.40	13	--	
F20	39	72	129	1.02	1.00	12	--	
F21	38	85	128	1.02	1.20	11	--	
F22	270	90	0	1.78	1.30	10	--	
F23	10	61	100	2.50	0.70	10	--	
F24	25	85	115	0.05	3.40	4	--	SW
F25	168	87	258	1.52	4.90	6	--	
F26	345	75	75	8.90	0.80	8	--	
F27A	222	77	312	0.70	1.60	5	--	
F27B	191	80	281	0.46	1.50	2	--	
F27C	210	80	300	0.05	7.50	1	--	
F28	45	86	135	0.13	0.50	14	--	
F29	38	85	128	2.50	0.50	5	--	
F30	97	89	187	-	0.60	12	--	O
F31	34	90	124	0.05	0.70	9	--	
F32	290	80	20	1.02	0.70	14	--	
F33	155	85	245	-	0.50	14	--	O
F34	74	78	164	6.40	0.50	10	--	
F35	34	81	124	3.80	1.30	10	--	
F36	32	77	122	0.05	0.60	10	--	
F37	23	77	113	0.05	0.60	10	--	SW
F38	218	82	308	0.10	2.30	5	--	SW
F39	287	56	17	8.89	6.50	13	--	
F40	34	90	124	1.91	6.90	3	--	
F41	37	82	127	27.90	1.30	8	--	
F42	32	67	122	8.90	1.20	9	--	
F43	225	77	315	0.05	1.00	9	--	
F44	210	83	300	0.05	1.10	10	--	
F45	212	84	302	0.05	0.70	9	--	
F46	208	75	298	0.05	1.00	10	--	
F47	305	90	35	0.64	0.80	8	--	
F48	5	85	95	0.13	13.30	9	--	SW
F49	16	78	106	15.20	5.80	8	--	
F50	25	86	115	1.02	1.40	10	--	SW
F51	119	77	209	0.76	0.70	8	--	
F52	275	85	5	-	0.40	12	--	O
F53	210	50	300	-	1.10	10	--	O
F54	185	84	275	0.10	4.40	9	--	SW

APPENDIX. Pavement 100, 200, and 300 --Continued

Fracture number	AZI	DIP	DIP DIR	Aperture (mm)	Length (m)	R.C.	Pitch	Remarks
			PAVEMENT 100--Continued					
F55	350	68	80	6.60	1.30	11	--	
F56	181	82	271	0.36	1.50	14	--	
F57	352	72	82	0.20	0.50	14	--	
F58	184	88	274	2.29	2.40	9	--	
F59	133	76	223	3.20	7.90	10	--	Fault
F60A	150	86	240	0.05	1.70	10	--	
F60B	170	87	260	1.60	4.80	10	--	
F61	329	87	59	6.40	1.70	11	--	
F62	322	82	52	0.05	2.20	10	--	
F63	330	56	60	0.51	1.20	11	--	
F64	330	51	60	0.51	2.10	10	--	
F65	153	78	243	0.20	3.60	8	--	SW
F66	150	87	240	18.30	8.80	8	--	
F67	7	75	97	2.50	2.00	7	--	
F68	349	89	79	0.05	0.80	14	--	
F69	162	82	252	3.80	1.10	10	--	
F70	168	65	258	1.52	2.30	9	--	
F71	90	79	180	3.60	1.90	10	--	
F72	358	72	88	0.05	1.90	9	--	
F73	338	72	68	4.60	2.30	16	--	
F74	11	89	101	1.65	4.70	123	--	
F75	200	87	290	0.89	0.90	12	--	
F76	10	87	100	0.05	0.50	12	--	
F77	9	79	99	0.05	0.80	14	--	
F78	149	84	239	0.20	1.20	14	--	
F79	200	83	290	0.13	7.80	9	--	
F80	15	85	105	0.05	0.70	15	--	
F81	13	80	103	0.12	0.90	4	--	
F82	342	70	72	-	1.30	-	--	O
F83	150	89	240	-	1.30	12	--	O
F84	6	52	96	12.20	1.50	15	--	
F85	350	61	80	0.04	2.80	14	--	SW
F86	38	70	128	0.04	3.70	16	--	
F87	200	86	290	0.08	3.90	13	--	SW
F88	134	78	224	6.40	2.80	14	--	
F89	120	84	210	24.10	1.50	4	--	
F90	182	78	272	-	0.50	11	--	O
F91	175	65	265	0.25	0.80	6	--	
F92	10	87	100	0.04	3.40	6	--	
F93	358	68	88	0.25	5.80	5	--	
F94	15	85	105	0.15	1.40	11	--	
F95	325	87	55	0.05	0.60	10	--	
F96	173	85	263	0.04	0.90	10	--	SW
F97	165	81	255	10.20	0.80	8	--	

APPENDIX. Pavement 100, 200, and 300 --Continued

Fracture number	AZI	DIP	DIP DIR	Aperture (mm)	Length (m)	R.C.	Pitch	Remarks
			PAVEMENT 100--Continued					
F98	340	90	70	12.70	0.70	9	--	
F99	325	82	55	2.80	1.30	8	--	
F100	175	76	265	0.51	2.30	10	--	
F101	120	80	210	2.50	1.80	8	--	
F102	135	88	225	0.13	0.70	12	--	
F103	20	90	110	0.41	1.20	14	--	
F104	75	86	165	5.10	0.70	6	--	
F105	155	77	245	6.40	3.10	9	--	Fault
F106	20	81	110	11.40	3.80	9	--	SW
F107	304	90	34	1.52	0.60	18	--	
F108	355	85	85	4.60	0.40	8	--	
F109	350	88	80	0.05	2.50	8	--	Fault
F110	174	80	264	0.38	0.80	10	--	SW
F111	113	66	203	0.25	1.70	8	--	
F112	224	75	3.14	0.04	1.20	6	--	SW
F113	105	71	195	1.14	0.80	12	--	SW
F114	322	86	52	2.50	2.60	14	--	
F115	357	82	87	0.28	0.70	9	--	
F116	76	79	166	0.38	0.80	10	--	
F117	322	88	52	0.05	0.50	13	--	
F118	326	82	56	0.28	1.20	12	--	
F119	325	87	55	33.00	0.80	10	--	
F120	135	59	225	21.30	0.80	13	--	
F121	352	90	82	-	0.60	9	--	O
F122	262	82	352	2.50	2.10	10	--	
F123	70	75	160	0.64	1.20	10	--	
F124	75	81	165	8.90	2.70	5	--	
F125	176	80	266	0.64	1.70	4	--	
F126	167	87	257	12.20	6.70	8	--	
F127	95	74	185	1.52	0.90	8	--	
F128	174	86	264	0.04	0.80	10	--	
F129	325	75	55	29.20	0.80	9	--	
F130	319	80	49	0.76	0.60	16	--	
F131	320	90	50	6.40	0.80	10	--	
F132	347	78	77	0.38	0.40	11	--	
F133	180	74	270	0.04	0.70	6	--	
F134	131	82	221	6.40	0.30	8	--	
F135	350	75	80	0.41	1.50	4	--	
F136	179	85	269	0.28	1.00	9	-	
F137	241	82	331	0.25	0.20	9	--	
F138	183	80	273	8.40	0.20	10	--	
F139	63	69	153	9.40	1.10	9	--	
F140	235	87	325	11.40	0.70	16	--	
F141	320	86	50	-	0.40	11	--	O
F142	63	79	153	3.30	1.50	12	--	

APPENDIX. Pavement 100, 200, and 300 --Continued

Fracture number	AZI	DIP	DIP DIR	Aperture (mm)	Length (m)	R.C.	Pitch	Remarks
			PAVEMENT 100--Continued					
F143	85	79	175	1.27	0.40	7	--	
F144	244	78	334	4.10	0.70	8	--	
F145	343	88	73	0.08	0.60	4	--	
F146	350	75	80	1.27	0.80	6	--	
F147	169	84	259	1.02	1.80	8	--	
F148	170	83	260	11.40	5.50	15	--	Fault
F149	263	87	353	12.70	0.80	11	--	
F150	132	81	222	2.29	2.20	5	--	
F151	305	80	35	0.28	1.30	9	--	
			PAVEMENT 200					
J1.1	221	76	311	0.04	2.40	1	14SW	
J1.2	215	87	305	0.56	10.80	2	15SW	PH
J2.1	216	76	306	0.65	3.00	1	13SW	
J2.2	215	76	305	0.04	16.40	1	14SW	
J3	212	63	302	0.95	16.60	4	-	PH
J4	218	86	308	6.40	18.40	2	14SW	PH
J5	219	75	309	0.04	2.60	1	-	PH
J6	165	79	255	-	0.50	3	-	O
J7	217	70	307	0.08	2.20	1	-	
F1	182	77	272	2.50	3.80	5	--	SW
F2	149	45	239	31.80	3.80	5	--	
F3	164	77	254	8.90	9.50	6	--	Fault
F4	45	76	135	8.90	0.90	6	--	
F5	170	84	260	2.50	3.90	4	--	
F6	334	58	64	0.56	1.25	12	--	
F7	325	68	55	0.64	1.70	16	--	
F8	350	62	80	0.56	1.50	9	--	
F9A	186	70	276	1.52	3.70	5	--	
F9B	155	45	245	0.10	1.40	-	--	
F10.1	145	58	235	0.04	2.90	8	--	
F10.2	149	61	239	0.04	0.90	10	--	
F11.1	274	87	4	0.08	2.30	4	--	
F11.2	270	84	0	0.04	3.40	9	--	
F12.1	105	81	195	0.25	12.60	9	--	
F12.2	121	87	211	0.46	0.90	13	--	
F13	143	57	233	0.04	1.10	10	--	
F14.1	150	54	240	0.38	2.90	6	--	
F14.2	358	90	88	0.27	1.80	7	--	
F15	33	87	123	0.04	8.80	8	--	SW
F16.1	280	75	370	8.00	0.20	10	--	
F16.2	260	75	350	1.27	3.70	12	--	
F17	228	72	318	0.04	8.10	11	--	SW
F18	115	75	205	0.56	11.10	12	--	

APPENDIX. Pavement 100, 200, and 300 --Continued

Fracture number	AZI	DIP	DIP DIR	Aperture (mm)	Length (m)	R.C.	Pitch	Remarks
			PAVEMENT 200--Continued					
F19	215	49	305	-	2.70	8	--	O
F20	88	88	178	6.40	11.80	12	--	
F21	155	87	245	0.64	3.00	12	--	SW
F22	174	80	264	0.04	1.60	9	--	
F23	178	86	268	0.04	2.00	12	--	
F24	171	55	261	0.04	2.10	13	--	
F25	178	78	268	0.04	1.50	8	--	
F26	345	80	75	0.10	3.00	10	--	
F27	346	89	76	0.51	3.00	10	--	
F28	135	65	225	0.43	0.80	10	--	
F29	270	86	0	12.20	3.70	10	--	
F30	320	51	50	-	0.60	14	--	O
F31	290	67	20	0.25	2.20	11	--	
F32	329	78	59	-	0.60	12	--	O
F33	152	32	242	-	1.40	12	--	O
F34	125	83	215	15.20	6.50	8	--	SW
F35	95	80	185	3.10	1.20	12	--	
F36	326	85	56	0.89	4.30	13	--	
F37	325	90	55	8.90	2.70	11	--	
F38	114	76	204	1.27	4.20	9	--	
F39	150	87	240	0.75	0.90	14	--	
F40	74	82	164	-	0.50	8	--	O
F41	100	85	190	12.70	1.50	10	--	
F42	318	69	48	0.10	1.00	8	--	
F43	170	80	260	0.05	6.70	12	--	SW
F44	265	80	355	0.28	4.60	14	--	
F45	270	76	0	0.04	1.30	12	--	
F46	182	88	272	1.02	15.70	12	--	
F47	35	90	125	1.27	2.40	8	--	
F48	359	76	89	2.50	3.40	5	--	
F49	350	87	80	1.27	7.00	10	--	
F50	161	79	251	0.66	1.30	9	--	
F51	348	88	78	0.15	5.80	8	--	
F52	154	75	244	1.02	1.50	7	--	
F53	167	86	257	0.04	1.80	17	--	
F54	160	77	250	8.90	7.00	6	--	
F55	40	90	130	0.04	3.90	6	--	SW
F56	197	84	287	0.04	15.10	8	--	SW
F57	238	89	328	6.40	4.70	5	--	
F58	245	65	335	25.40	2.50	6	--	
F59	257	84	347	0.18	0.60	9	--	
F60	64	90	154	6.40	2.30	8	--	
F61	315	68	45	0.76	0.40	15	--	
F62	85	90	175	0.20	0.40	5	--	

APPENDIX. Pavement 100, 200, and 300 --Continued

Fracture number	AZI	DIP	DIP DIR	Aperture (mm)	Length (m)	R.C.	Pitch	Remarks
			PAVEMENT 200--Continued					
F63	75	78	165	21.60	0.80	6	--	
F64	135	57	225	0.56	0.70	15	--	
F65	46	90	136	12.20	2.30	6	--	
F66	58	84	148	3.10	2.30	6	--	
F67	34	76	124	-	1.30	8	--	O, SW
F68	175	68	265	0.04	0.40	14	--	
F69	178	78	268	-	3.00	9	--	O
F70A	285	88	15	0.31	2.80	10	--	
F70B	265	84	355	0.64	0.70	8	--	
F71	16	87	106	0.76	2.20	12	--	
F72	270	85	0	0.13	0.50	11	--	
F73	246	81	336	0.04	0.40	12	--	
F74	25	90	115	0.20	0.35	12	--	
F75	78	83	168	1.24	0.90	6	--	
F76	108	87	198	8.90	7.00	14	--	
F77	335	88	65	0.89	2.70	10	--	
F78	345	90	75	0.51	1.30	11	--	
F79	125	87	215	0.56	5.70	12	--	
F80	60	85	150	0.04	1.20	12	--	
F81	242	80	332	0.64	1.20	12	--	
F82	100	74	190	0.04	0.90	12	--	
F83	168	75	258	0.04	3.60	14	--	
F84	163	88	253	0.04	1.10	11	--	
F85	167	76	257	0.15	1.20	6	--	
F86	112	85	202	1.27	3.20	10	--	
F87	164	84	254	0.04	1.20	8	--	
F88	305	72	35	0.04	2.50	13	--	
F89	61	90	151	1.00	2.30	10	--	
			PAVEMENT 300					
J1	315	83	45	3.10	5.30	4	8SE	
J2	135	82	225	9.40	1.30	2	28SE	
J3.1	204	77	294	8.90	2.00	2	14SW	
J3.2	210	73	300	-	0.40	2	15SW	O
J4	317	81	47	8.90	7.40	1	18SE	
J5	321	78	51	12.20	5.40	3	19SE	
J6	179	79	269	0.04	0.70	-	-	
J7	211	79	301	2.50	2.20	2	14SW	
J8	310	85	40	0.04	0.40	3	14SE	
J9A	309	82	39	0.04	2.70	1	10SE	PH
J9B	320	80	50	0.04	3.70	4	20SE	
J10	331	74	61	12.20	0.80	3	27SE	
J11	314	84	44	15.00	5.00	1	12SE	O, PH
J12	316	70	46	8.90	0.50	3	20SE	

APPENDIX. Pavement 100, 200, and 300 --Continued

Fracture number	AZI	DIP	DIP DIR	Aperture (mm)	Length (m)	R.C.	Pitch	Remarks
			PAVEMENT 300--Continued					
J13	347	81	77	4.10	0.70	-	22SE	
J14	307	80	37	10.20	0.50	3	37SE	
J15	145	82	235	3.10	8.80	-	50SE	
J16	201	81	291	0.04	1.30	4	15SW	PH
J17A	312	86	42	0.04	1.25	1	26SE	PH
J17B	326	87	56	0.50	6.25	2	43SE	
J18	319	88	49	0.04	8.20	-	18SE	11SE
J19	224	71	314	0.00	0.80	2	18SE	H
J20	330	84	60	0.04	7.80	2	38SE	
J21	223	85	313	19.10	0.30	2	7SW	
J22	317	80	47	0.00	0.30	-	-	H
J23	317	87	47	2.41	2.30	2	10SE	
J24	321	78	51	1.91	4.80	1	26SE	
J25	220	78	310	0.13	2.70	1	25SW	
J26	317	83	47	0.04	13.10	3	21SE	46SE, PH
J27	345	85	75	0.00	6.50	-	23SE	H
J28	312	88	42	0.13	0.90	1	36SE	
J29	216	72	306	0.04	1.00	1	-	PH
J30A	311	83	41	0.04	2.20	1	33SE	
J30B	325	79	55	0.04	9.75	2	34SE	
J31	35	90	125	7.90	0.30	4	41SW	
J32	355	78	85	0.05	2.50	2	17SE	
J33	320	78	50	9.10	1.60	2	48SE	
J34	0	76	90	0.51	3.00	-	-	PH
J35	165	78	255	0.51	1.40	2	38SE	
J37	324	85	54	0.25	3.20	1	40SE	
J36B	301	86	31	0.31	2.50	1	43SE	PH
J37	240	86	330	-	0.30	2	17SE	O
J38	330	86	60	0.76	1.40	2	46SE	
J39	219	77	309	0.36	3.20	2	19SE	11SW
J40	320	78	50	2.03	0.70	3	40SE	
J41	320	82	50	0.08	0.50	3	51SE	
J42	310	81	40	0.76	0.50	4	-	
J43	220	76	310	0.04	1.40	3	-	
J44	331	87	61	-	2.60	1	19SE	O, 29SE
J45	45	90	135	-	1.40	4	17SE	O
J46.1	210	71	300	-	1.90	1	47SW	O
J46.2	205	76	295	-	0.60	2	48SW	O
J47	204	76	294	3.30	1.50	-	17SW	
F1	200	70	290	0.04	0.80	14	--	
F2	46	81	136	0.64	1.90	9	--	
F3	45	90	135	0.25	0.50	7	--	
F4	356	90	86	0.04	0.50	7	--	
F5	173	75	263	0.38	1.30	9	--	

APPENDIX. Pavement 100, 200, and 300 --Continued

Fracture number	AZI	DIP	DIP DIR	Aperture (mm)	Length (m)	R.C.	Pitch	Remarks
			PAVEMENT 300--Continued					
F6	49	56	139	0.76	0.50	10	--	
F7	178	71	268	0.04	1.40	10	--	
F8	62	90	152	3.20	4.30	6	--	
F9A	190	65	280	0.76	1.10	14	--	
F9B	154	60	244	-	1.50	-	--	O
F10	187	67	277	10.70	0.90	12	--	
F11	160	82	250	6.40	2.70	11	--	
F12	171	79	261	12.70	1.70	9	--	
F13	135	58	225	0.04	1.20	7	--	
F14	50	76	140	1.40	1.20	7	--	
F15	243	74	333	-	1.30	8	--	O
F16	235	84	325	-	1.30	6	--	O
F17	331	90	61	-	0.90	6	--	O
F18	339	90	69	1.27	5.60	10	--	SW
F19	194	64	284	1.30	0.40	12	--	
F20	187	59	277	1.50	0.90	-	--	
F21	187	80	277	0.89	0.40	13	--	
F22	193	72	283	-	0.60	8	--	O
F23	205	74	295	-	0.30	8	--	O
F24	206	85	296	2.46	0.30	8	--	
F25	211	79	301	1.27	0.80	12	--	
F26	43	90	133	0.05	0.30	12	--	
F27	325	90	55	-	0.60	6	--	O
F28	143	84	233	-	0.40	6	--	O
F29	136	79	226	0.89	0.50	7	--	
F30	314	90	44	1.70	0.70	7	--	
F31	335	90	65	1.40	2.50	12	--	
F32A	234	72	324	0.51	1.10	11	--	
F32B	332	87	62	0.38	0.60	-	--	
F33	155	78	245	6.40	2.70	6	--	
F34	76	77	166	0.76	1.20	8	--	
F35	20	90	110	6.40	0.80	8	--	
F36	347	90	77	0.04	0.90	9	--	SW
F37	155	75	245	2.80	1.10	4	--	
F38	161	89	251	-	1.70	5	--	O
F39	114	67	204	0.38	0.60	10	--	
F40	198	80	288	5.10	1.70	5	--	
F41	60	77	150	6.40	1.80	12	--	
F42	25	81	115	-	2.10	13	--	O
F43	155	44	245	-	1.70	9	--	O
F44	69	78	159	1.47	1.60	12	--	
F45	57	83	147	0.89	1.50	14	--	
F46	151	85	241	2.29	3.80	6	--	
F47	39	54	129	3.80	2.40	13	--	

APPENDIX. Pavement 100, 200, and 300 --Continued

Fracture number	AZI	DIP	DIP DIR	Aperture (mm)	Length (m)	R.C.	Pitch	Remarks
			PAVEMENT 300--Continued					
F48	140	49	230	-	0.90	9	--	O
F49	147	53	237	1.02	1.70	5	--	
F50	149	70	239	0.04	0.80	9	--	
F51	351	85	81	0.38	0.80	9	--	
F52	358	84	88	0.64	2.30	8	--	SW
F53	235	70	325	1.91	0.70	13	--	
F54	278	81	8	0.25	0.60	14	--	
F55	124	59	214	0.89	1.20	6	--	
F56	179	80	269	6.40	0.80	14	--	
F57	250	86	340	2.34	0.80	10	--	
F58	210	66	300	3.20	1.30	10	--	
F59	45	55	135	2.03	0.80	14	--	
F60	17	84	107	1.52	0.70	10	--	
F61	218	82	308	1.78	1.30	11	--	
F62	320	90	50	2.50	3.60	11	--	
F63	50	89	140	-	0.50	12	--	O
F64	148	56	238	1.65	3.30	6	--	
F65	331	90	61	-	0.80	12	--	O
F66	45	84	135	0.25	0.70	13	--	
F67	348	87	78	-	0.80	13	--	O
F68	38	90	128	0.25	1.20	17	--	
F69	210	85	300	0.36	1.20	9	--	
F70	19	76	109	0.56	0.50	14	--	
F71	35	90	125	6.40	1.60	16	--	
F72	133	40	223	-	5.50	9	--	O
F73	70	86	160	31.80	0.80	10	--	
F74	20	86	110	0.25	0.90	16	--	
F75	174	81	264	1.27	1.30	11	--	
F76	230	88	320	6.40	1.40	14	--	
F77	150	79	240	0.64	1.90	12	--	SW
F78	11	63	101	0.20	0.60	16	--	
F79	326	84	56	0.04	0.60	4	--	
F80	322	83	52	0.04	0.50	6	--	
F81	320	78	50	0.25	0.80	11	--	
F82	29	84	119	0.94	1.10	13	--	SW
F83	330	90	60	0.76	2.50	4	--	
F84	20	90	110	0.25	1.80	17	--	
F85	239	82	329	0.04	2.50	16	--	
F86	59	68	149	0.64	0.70	14	--	
F87	53	68	143	0.13	1.00	12	--	
F88	35	90	125	6.40	3.60	14	--	
F89	28	78	118	6.40	2.00	15	--	
F90	218	75	308	8.90	2.90	16	--	
F91A	55	90	145	2.41	1.20	16	--	

APPENDIX. Pavement 100, 200, and 300 --Continued

Fracture number	AZI	DIP	DIP DIR	Aperture (mm)	Length (m)	R.C.	Pitch	Remarks
			PAVEMENT 300--Continued					
F91B	212	82	302	-	1.50	-	--	O
F92	50	82	140	22.90	0.60	16	--	
F93	339	76	69	6.40	1.30	12	--	
F94	15	78	105	0.13	2.30	16	--	SW
F95	57	80	147	0.64	0.80	9	--	
F96	15	57	105	3.20	1.10	10	--	
F97	132	86	222	0.51	4.50	9	--	
F98	322	80	52	1.52	2.80	9	--	
F99	355	90	85	1.65	2.50	8	--	
F100	180	89	270	3.10	2.70	6	--	
F101	358	90	88	2.50	1.00	13	--	SW
F102	145	47	235	0.64	3.40	8	--	
F103	192	83	282	1.02	2.30	6	--	SW
F104	45	90	135	-	1.20	17	--	O
F105	208	74	298	0.38	0.90	14	--	
F106	300	90	30	0.53	1.30	10	--	
F107	342	90	72	0.51	0.70	6	--	
F108	348	90	78	-	0.90	12	--	O
F109	156	85	246	0.04	0.60	5	--	
F110	340	90	70	0.89	0.50	9	--	
F111	139	50	229	0.64	1.90	5	--	
F112	245	87	335	38.10	2.30	10	--	
F113	330	81	60	0.04	13.70	6	--	SW
F114	198	68	288	-	0.70	5	--	O
F115	29	80	119	0.04	0.80	8	--	
F116	196	79	286	21.10	1.30	10	--	
F117	327	90	57	-	0.40	10	--	O
F118	161	77	251	-	0.70	5	--	O
F119	124	88	214	5.30	3.10	6	--	
F120	33	45	123	50.80	1.80	10	--	
F121	118	80	208	0.38	1.60	10	--	SW
F122	322	80	52	-	1.50	5	--	O
F123	329	83	59	0.13	13.00	5	--	SW
F124	324	81	54	0.13	1.60	9	--	
F125A	334	74	64	0.43	1.50	8	--	
F125B	320	79	50	0.28	1.90	10	--	
F126	330	84	60	1.52	3.00	12	--	
F127	322	88	52	0.25	1.10	12	--	
F128	311	75	41	0.56	1.20	9	--	
F129	0	70	90	0.25	2.30	10	--	
F130	340	70	70	0.76	1.80	12	--	
F131	318	74	48	0.04	0.50	9	--	
F132	320	90	50	0.38	4.10	14	--	
F133	351	90	81	0.20	0.90	8	--	

APPENDIX. Pavement 100, 200, and 300 --Continued

Fracture number	AZI	DIP	DIP DIR	Aperture (mm)	Length (m)	R.C.	Pitch	Remarks
			PAVEMENT 300--Continued					
F134	232	77	322	46.00	0.40	14	--	
F135	330	79	60	0.04	3.20	13	--	
F136	130	76	220	-	3.80	5	--	O, Fault
F137	120	77	210	1.02	5.70	13	--	
F138	150	82	240	0.04	0.90	14	--	
F139	143	63	233	0.20	1.40	10	--	
F140	323	83	53	0.64	1.40	10	--	
F141	330	90	60	0.04	5.00	7	--	
F142	321	87	51	0.04	2.30	9	--	
F143	327	89	57	0.91	1.00	14	--	
F144	329	80	59	0.04	5.00	12	--	
F145	326	82	56	0.25	3.50	9	--	SW
F146	324	83	54	0.38	2.40	8	--	
F147	60	79	150	6.40	3.00	17	--	
F148	150	81	240	0.41	0.90	9	--	
F149	305	90	35	0.36	0.80	13	--	
F150	169	75	259	0.18	0.50	14	--	
F151	174	80	264	0.81	1.10	13	--	
F152	53	90	143	1.52	0.80	12	--	
F153	37	85	127	0.76	1.30	14	--	
F154	249	75	339	0.51	0.80	12	--	
F155	80	63	170	0.20	1.20	13	--	
F156	304	84	34	0.86	6.50	4	--	
F157	300	90	30	0.81	2.70	9	--	
F158	40	90	130	0.25	0.50	16	--	
F159	43	80	133	0.04	0.60	5	--	
F160	31	90	121	0.04	0.30	5	--	
F161	225	68	315	0.25	0.80	12	--	
F162	215	75	305	0.20	1.20	12	--	
F163	198	88	288	0.13	0.60	10	--	
F164	331	85	61	-	5.70	12	--	O
F165	156	81	246	-	2.00	4	--	O
F166	151	79	241	25.40	7.20	6	--	
F167	201	70	291	-	1.50	6	--	O
F168	305	90	35	0.04	0.40	14	--	
F169	169	69	259	0.15	1.60	9	--	
F170	210	72	300	5.80	0.40	8	--	
F171	94	85	184	0.25	3.90	18	--	SW
F172	354	60	84	0.23	1.00	15	--	
F173	2	73	92	0.25	0.80	14	--	
F174	355	64	85	0.08	2.80	10	--	
F175	345	90	75	0.04	1.10	18	--	
F176	2	72	92	0.04	1.20	10	--	
F177	5	66	95	0.13	1.30	18	--	

APPENDIX. Pavement 100, 200, and 300 --Continued

Fracture number	AZI	DIP	DIP DIR	Aperture (mm)	Length (m)	R.C.	Pitch	Remarks
			PAVEMENT 300--Continued					
F178	350	90	80	0.04	3.60	12	--	SW
F179	3	83	93	0.38	3.50	8	--	
F180	0	90	90	0.04	6.70	8	--	
F181	155	67	245	0.04	2.10	14	--	
F182	25	90	115	0.04	0.70	12	--	
F183	55	78	145	0.05	1.30	12	--	
F184	357	87	87	0.31	2.40	13	--	
F185	298	90	28	0.20	2.40	12	--	
F186	60	90	150	0.46	1.20	11	--	
F187	180	89	270	0.05	1.70	12	--	SW
F188	125	71	215	0.04	2.90	10	--	
F189	304	90	34	-	2.00	8	--	O
F190	240	78	330	30.50	1.70	8	--	
F191	90	90	180	0.04	2.40	10	--	
F192	280	90	10	0.05	4.90	6	--	
F193	120	74	210	0.51	3.70	12	--	
F194	45	90	135	0.08	3.10	13	--	
F195	155	70	245	0.08	2.30	9	--	
F196	11	80	101	0.05	1.60	9	--	
F197	13	81	103	0.04	0.90	-	--	
F198	25	85	115	0.05	2.20	12	--	
F199	40	65	130	0.97	1.40	14	--	
F200	164	78	254	0.10	1.30	8	--	

☆U.S. GOVERNMENT PRINTING OFFICE. 1994-0-575-003